ADVANCED MATERIALS TECHNOLOGIES
www.advmattechnol.de

Precise Control of Interfacial Charge Transport for Building Functional Optoelectronic Devices

*Weining Zhang, Hongliang Chen, and Xuefeng Guo**

Optoelectronic devices and interfaces therein have captured great attention in both scientific and industrial communities because of the wide variety of their unique properties. From a materials chemistry point of view, each layer and individual component of an optoelectronic device possesses the possibility of flexible chemical modification, making it feasible to dope, mix, and physically/chemically modify the interface. Exploiting the novel properties in optoelectronic devices with diverse layerings of metals, semiconductors, and insulators, along with the interfaces between them, leads to new electronic device designs, including functional transistors, biodetection devices, and flexible electronics, as well as other types of traditional optoelectronic devices, such as photodetectors, photovoltaic devices, and light-emitting devices, with unprecedented characteristics or unique functionalities. This article reviews the recent developments and challenges and provides a perspective on the exploration of interface-engineered organic optoelectronic devices for future applications in electronics and optoelectronics.

1. Introduction

Device performance is primarily dependent on the nature of the materials used and the respective interface between two materials. **Figure 1**a,b presents the typical interface topics in field-effect transistors (FETs) and solar cells, including but not limited to: 1) regulating the surface work function of the electrode, 2) functionalizing the electrode surface, 3) reducing the surface roughness and structural defects of the dielectric layer, 4) reducing the traps on the surface of the dielectric layer, 5) functionalizing the surface of the dielectric layer, 6) controlling the charge transfer at the semiconductor/environment interface, and 7) adjusting the photogenerated carrier transport at the ternary interface. These heterogeneous interface engineering studies have not only improved device performance, but have even built novel functions. At present, interface engineering has become a research hotspot and has great potential for further applications in diverse fields, ranging from integrated circuits and energy conversion to catalysis and chemical/biosensors. Scientists with various backgrounds have been devoting great efforts to this area, which has moved from the simple improvement of device performance to branch out in broad directions, indicating its interdisciplinarity.

As shown in Figure 1c, an important interface for an FET is the semiconductor/electrode interface, which typically determines the efficiency of charge carrier injection and extraction. In general, the charge injection of a metal/organic semiconductor (OSC) junction can be described in terms of thermal electron emission or tunneling mechanisms, depending on the concentration of defect states inside the bandgap (Figure 1c, left and middle).[1] By carefully selecting the self-assembled monolayer (SAM) or thin buffer interlayer to modify the metal electrode (Figure 1c, right), the interface charge injection barrier can be fine-tuned, thereby significantly reducing the contact resistance of the device. More interestingly, by using a stimuli-responsive conformational isomer as a functional layer to modify the electrode interface, functionalization of the electrodes can be achieved. This concept laid the foundation for the construction of functional devices such as optical/electrical switches, memory, and photodetectors.

The semiconductor/dielectric interface is another important interface in FETs, that governs carrier transport (Figure 1d, left), because generation, transport, and regulation of charge carriers all occur in the first few layers (<10 nm) of semiconductors at the interface (Figure 1d, middle). In addition, the modification of the dielectric surface has been shown to help reduce the defects, improve the roughness, change the polarity, and modulate the surface hydrophilic/hydrophobic properties. These changes further affect the transport of carriers at the semiconductor/dielectric interface (Figure 1d, right) and have a significant impact on the morphology of the semiconductor layer. Furthermore, modification of the interface with SAMs or stimuli-responsive layers offers an important and general methodology to improve device performance and even integrate new molecular functionalities, such as photocontrollable memory, superconductivity, and charge-trap memory, into organic electrical circuits.

W. Zhang, Dr. H. Chen, Prof. X. Guo
Beijing National Laboratory for Molecular Sciences
State Key Laboratory for Structural Chemistry of Unstable and Stable Species
College of Chemistry and Molecular Engineering
Peking University
Beijing 100871, P. R. China
E-mail: guoxf@pku.edu.cn
Prof. X. Guo
Department of Materials Science and Engineering
College of Engineering
Peking University
Beijing 100871, P. R. China

DOI: 10.1002/admt.201800358

Recently, we[2–14] and some other groups[15–19] found that more efficient functional and hybrid devices can be realized by building more complicated ternary interfaces (Figure 1e) such as semiconductor/recognition receptor/environment interfaces for specific light/chemistry/biosensing (Figure 1e, left), or a dye/single layer graphene (SLG)/titanium oxide (TiO_2) ternary interface, for efficient charge transport and photovoltaic conversion (Figure 1e, middle and right). The key to this idea is to separate the signal recognition from charge transport, each performing its own functions without interfering with the other. Typically, the semiconductor/environment interface can be used to construct FET-based sensors by directly exposing the semiconductor layer to the environment being analyzed. This sensing mechanism can be attributed to the diffusion of the analyte into the grain boundaries of the semiconductor, resulting in the trapping or doping of charge carriers. However, this method is generally less selective and specific, and can lead to serious problems with device stability and reversibility, due to physical destructive interactions between the semiconductor and analyte. Therefore, by reasonably introducing a receptor that has a specific response to the analyte, at the semiconductor/environment interface, both recognition and charge transport can be performed at the interface by the acceptor and semiconductor, respectively, which effectively controls the doping effect and improves the sensing selectivity/sensitivity.

In this review, we focus on the modification, integration, properties, and applications of important interfaces in optoelectronic devices. Since there are many reviews related to this topic,[1,20–26] we only summarize our recent advances and those of others related to interface-engineered optoelectronic devices. First, we briefly introduce some common interface modification strategies and review their intrinsic chemistry, applicable objectives, and conditions of use. Then, we summarize the typical works of modifying and functionalizing binary interfaces in FETs by doping, insertion, and physical or chemical modification. Finally, we discuss the novel electronic and optical properties of the ternary interface of hybrid optoelectronic devices. This enables the creation of a variety of ultrathin, flexible, and transparent electronic and optoelectronic devices, including vertical FETs, pressure sensors, wearable and biocompatible electronic devices, photodetectors, solar cells, and light-emitting devices (LEDs).

Weining Zhang received his B.S. degree in 2014 from the School of Chemistry and Chemical Engineering, Shandong University. He is currently working toward a Ph.D. degree in Chemistry at the College of Chemistry and Molecular Engineering, Peking University, under the guidance of Prof. Xuefeng Guo. His current research is focused on organic optoelectronics.

Hongliang Chen received his Ph.D. in 2016 from the College of Chemistry and Molecular Engineering, Peking University under the guidance of Prof. Xuefeng Guo. From 2016 to 2018, he was a research scientist in Dow Chemical Company. He is currently a postdoctoral fellow at Northwestern University, USA, where his research interest is focused on organic functional devices.

Xuefeng Guo received his Ph.D. in 2004 from the Institute of Chemistry, Chinese Academy of Sciences, Beijing. From 2004 to 2007, he was a postdoctoral research scientist at the Columbia University Nanocenter. He joined the faculty as a professor under the "Peking 100-Talent" Program at Peking University in 2008. His research is focused on functional nanometer/molecular devices.

2. Interface Modification Methods

In this section, we discuss the methods developed for modifying the surfaces of electrodes and dielectrics. Since there are already many comments in this field, we do not go into details, but just review the recent developments and challenges.

2.1. Electrode Modification

Gold is the one of the most commonly used electrode materials in organic electronics because of its inertness under ambient conditions. Moreover, the work function of Au well matches the energy level of OSCs, resulting in lower contact resistance. Other metal electrodes show interesting electronic properties as well. For example, a metal with an ultrahigh or ultralow work function can be used to construct Ohmic contacts with special semiconductors. Furthermore, asymmetric electrodes with different work functions can be used as photogenerated carrier collectors. However, many of these metals easily oxidize in air, creating insulating layers on the surface, which prevent the formation of clean metal/OSC contacts. Handling them under ultrahigh vacuum or inert gas conditions can help avoid this problem, but increases the complexity of the experiments.

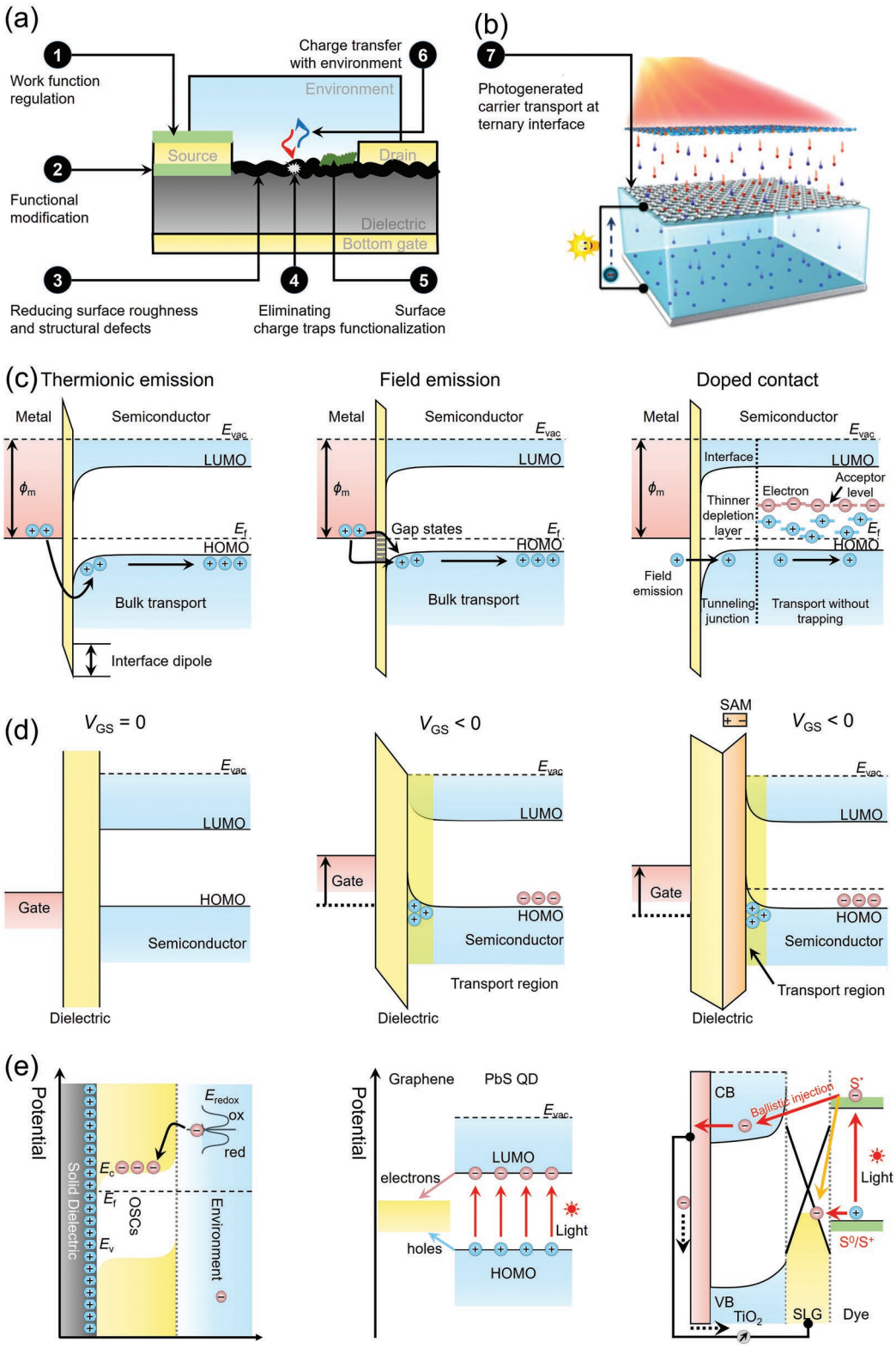

Figure 1. Interfacial effects in optoelectronic devices. Typical interfaces in a) field-effect transistors and b) solar cells. c) Schematic illustration showing the electrode/semiconductor interface injection governed by thermionic emission (left), field emission (tunneling) (middle), and electrode doping controlled tunneling process (left). d) Schematic illustration showing the energy level alignments at semiconductor/dielectric interfaces when $V_{GS} = 0$ (left), $V_{GS} < 0$ (p-type semiconductor) (middle), and SAM modified interfaces (right). e) Schematic illustration showing charge transfer at a ternary interface. E_f: Fermi level, E_{vac}: vacuum level, ϕ_m: work function of metal, HOMO: highest occupied molecular orbital, LUMO: lowest unoccupied molecular orbital. (b) Reproduced with permission.[13] Copyright 2016, American Chemical Society. (c) Adapted with permission.[1] Copyright 2015, ScienceDirect.

(a)

	Non–covalent anchor	Covalent anchor
Electrode (Au, Ag, CNT, Graphene)	Metal oxides: MoO_3, TiO_2, WO_3… Metal salts: LiF, NaCl… Small molecules: TCNQ…	Au-S: —SH —SMe —SOAc -S-S-  Au-C: Me_3Sn- Me_3Si—≡- $^+N{=}N$- 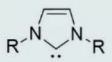
Dielectric (SiO_2, AlO_x, HfO_x)	Covered with polymer dielectric BCB, PVA, PMMA	SiO_2: -$SiCl_3$ -$Si(OCH_3)_3$ 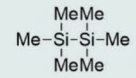 High-*k* dielectric: -COOH 

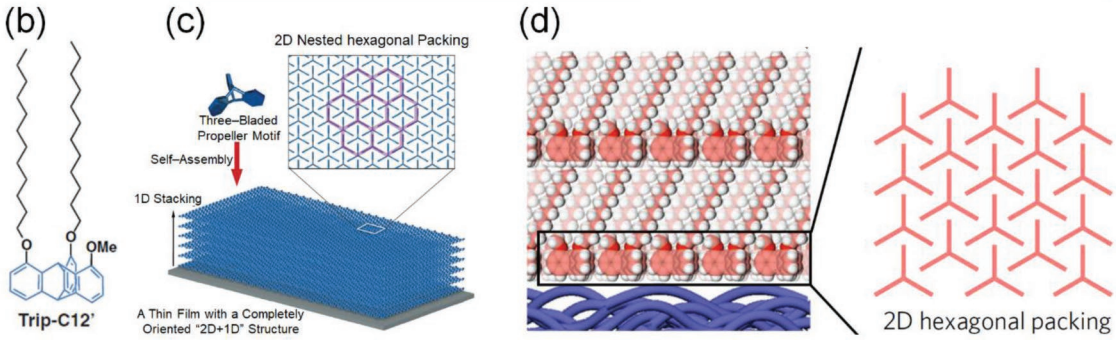

Figure 2. Electrode and dielectric modification strategies. a) Noncovalent and covalent anchors which include inorganics, organic small molecules, and polymers to modify metal electrodes and metal oxide dielectrics. b) Triptycene molecule used to functionalize solid polymer substrates. c) Schematic illustration of three-bladed, propeller-shaped triptycene molecules forming a 2D hexagonal array. It stacks 1D to form multilayers (oriented "2D + 1D" structure) with a long-range order. d) Schematic illustration of the 2D nested hexagonal packing of triptycene on polymer substrates. (b,c) Reproduced with permission.[27] American Association for the Advancement of Science. (d) Reproduced with permission.[28] Copyright 2018, Nature Publishing Group.

Recently, carbon nanomaterials, such as single-walled carbon nanotubes (SWCNTs) and graphene, have attracted great attention because of their high electrical conductivity, high chemical stability, and simple bottom-up preparation methods. Another significant feature of SWCNTs and graphene is that they are entirely composed of conjugated aromatics that are intrinsically the same building blocks as those of OSCs. This structure compatibility provides a solid structural basis for carbon nanomaterial/OSC contacts.

Anchoring groups (anchors, also known as linking groups or contact groups) mechanically and electronically attach a monolayer of molecules to the electrodes. Anchoring groups typically bind to electrodes covalently or via physical interactions. We have listed, in **Figure 2**a, the prototypical anchors for different electrode–anchor interactions.

Physical modifications involve the insertion of a buffer interlayer at metal electrode/OSC interfaces. Commonly employed interlayers include metal oxides,[29–32] metal salts,[33–36] and organic compounds.[24,37–39] Metal oxides provide a variety of candidates because of their wide range of work functions ranging from very low (ϕ = ≈3 eV for ZrO_2) to extremely high (ϕ = ≈7 eV for V_2O_5).[40,41] Metal salts are another big family of inorganic materials working as buffer interlayers that experience a similar mechanism as that by metal oxides. In addition, the doping effect also plays an important role when the interlayer component is capable of interacting with the active channel materials at the modified-metal/OSC interface.[24] When it comes to small organic molecules as an insertion layer, sometimes, direct charge transfer occurs at the interface between the interlayer and semiconductor, which helps to reduce the contact resistance, through the additional interface dipole.[42–44] On many occasions, small-molecule modification functions depend on the molecular contact doping effect.

Covalent contacts are more valuable and have been widely studied because they provide a more precisely controlled contact between molecules and electrodes. They are physically robust and electronically strong connections that can couple the behavior of molecules and electrodes. Among them, the Au—S linkages, formed from the reduction of thiol (—SH) anchors on Au surfaces, are the most widely adopted. Strong Au—S contacts enable the self-assembled monolayer to withstand harsh external conditions such as chemical processing, high-bias voltage measurements, and mechanical stress during

real applications.[45–47] However, under ambient conditions, thiols can be easily oxidized to disulfides (S—S bonds). S—S bonds are usually regarded as the "weak links" in many molecules and can be reduced on gold surfaces.[48–50] The most common preparations of disulfides to modify gold are either that breaking of a dimer linked with S—S bonds or immobilizing with a lipoic acid (thioctic acid) linker. In addition, to improve the ambient stability, functionalization of the thiol-based molecules with thioacetate or methyl-protecting groups is another common method.[51–53]

Nevertheless, the Au—S bond is not completely inert, and the oxidative and thermal stability of thiol-functionalized SAMs is far from perfect. The Au—C contact is one of the most promising covalent interactions on account of its chemical stability and rich selectivity. We list below three general methods for in situ generation of Au—C covalent contacts. The first method adopts the reactivity of C—SnR_3 bonds based on transmetalation to generate Au—C bonds on gold surfaces.[54,55] However, this approach uses and produces toxic and volatile trimethyltin species, which limits its wide application. The second method involves the deprotection of trimethylsilyl (TMS) end groups. Adding tetrabutylammonium fluoride to a TMS solution selectively cleaves the terminal ethynyl—Si bonds, and the target molecules attach to the gold surface. This approach has been used to fabricate single-molecule break junctions with Au tips.[56] The third method to produce covalent Au—C contacts is to electrochemically reduce diazonium salts.[57] However, diazonium salts are thermally unstable and explosive in many circumstances, which limits the universality of this method.

Recently, *N*-heterocyclic carbenes (NHCs) emerged as a versatile surface modification of the gold surfaces, in contrast to the most commonly used linear organosulfur ligands.[58–60] NHCs are versatile and reactive intermediates stabilized through at least one nitrogen next to the carbene functional group within the heterocyclic ring structure. They have gained increasing attention in the area of surface chemistry, on account of the following reasons: 1) their ability to form strong covalent bonds with metallic surfaces; 2) further stabilization of the singlet carbene state by the cyclic NHC structure, which forms an sp^2-like arrangement, resulting in C—N bonds with a partial double-bond character; 3) the broad structural variety of NHCs contrasting with that of thiol ligands, whose interfacial properties are mainly determined by the head group of the alkyl chain, as a consequence of close packing within the SAM.[61] Thus, planar gold surfaces functionalized with NHCs are easily tunable and more diverse, providing new modifications and applications of metallic gold in nanotechnology.

Despite this progress, there are still many unsolved issues in the implementation of covalent modification of metal electrodes. Moreover, the stability, mechanical performance, and scratch resistance of SAMs remain great challenges for practical uses and industrial applications. Carbon nanomaterials, such as carbon nanotubes (CNTs) and graphene, have emerged as highly conductive and stable carbon electrodes.[62] However, their chemical inertness makes them hard to functionalize without breaking the well-defined structure and scarifying their conductivity. Moreover, the mass-production, purification, and integration of carbon nanomaterials as electrodes is a huge systematic project. There is still a long way to go.

2.2. Dielectric Modification

SAM modification using long-chain organosilanes ($RSiX_3$ structure, see Figure 2a) is a general and powerful strategy to reduce the number of electron-trapping sites (mostly hydroxyl dangling groups) on the SiO_2 surface. The driving force for the on-surface self-assembly of organosilanes is the reactivity of anchors (Si—Cl, Si—OMe, etc.) with surface silanol (—Si—OH) to form strong Si—O—Si bonds, connecting the target silane to the surface.[63] Figure 2a illustrates the chemical structures of commonly used silane anchors. Different functions of the SAM can be realized by selectively choosing target tail such as alkane chains (octyltrichlorosilane, referred to as OTS, and octadecyltrichlorosilane), hexamethyldisilazane, hydrophobic and electron-withdrawing perfluoroalkylsilanes, and electron-donating amine-terminated alkylsilanes. The packing and ordering of the chemisorbed organosilanes are determined by the underlying siloxane network, interchain interactions, and reaction temperature.[64]

In addition, the dipole moment of the SAM at the OSC/dielectric interface affects the charge transport behavior.[65–67] For example, Kobayashi et al.[65] found that the carrier density in bottom-gate organic FETs (OFETs) could be affected by organosilane SAMs; holes and electrons could be accumulated by fluorine- and amino-substituted SAMs, respectively. Boudinet et al.[66] reported that chemical functionalization of the substrate by using SAMs with different end groups also had a significant influence on the performance of top-gate OFETs, such as dramatic variations in the threshold voltage and ON/OFF ratio.

However, on most occasions, SAMs cannot eliminate all the surface SiOH groups because of the limited reactivity of surface chemistry. Moreover, an ultrathin SAM (<2 nm) may cause charge-carrier tunneling under a high voltage.[68–72] In this case, inserting a layer can solve these problems. By depositing an ultrathin layer of calcium onto the surface of a gate dielectric, as an interfacial doping layer, the Ca thin layer could become oxidized to form —CaOH and —CaO, providing an additional dielectric layer as passivation. This could eliminate the surface traps because of the ionic binding nature of —CaOH, whereby Ca atoms could donate electrons and thus neutralize the hydroxyl groups.[73,74] Furthermore, appropriate hydroxyl-free polymers, such as a divinyl-tetramethylsiloxane-bis(benzocyclobutene) derivative,[75] can also be used as surface modifiers on SiO_2 dielectrics to achieve better n-type charge-transport behaviors in conjugated polymers.[76] In fact, polymer coating has been demonstrated as a powerful method to modify the dielectric surface and improve the performance of OFETs.[77] For example, Kim et al.[78,79] reported that the performance of pentacene FETs with a bottom-gate top-contact (BGTC) configuration could be modulated by changing the surface conditions of a polymer dielectric with different molecular structures due to their influence on the grain size/crystallinity of pentacene films.

High-*k* materials include different kinds of compounds, such as the most abundant inorganic oxides[80–82] and polymers,[83–85] as well as hybrid dielectrics.[86–88] Herein, we focus on inorganic oxide-based high-*k* materials (such as HfO_2, Al_2O_3, and ZrO_2). Organophosphonate SAMs have been easily prepared

under air and form well-ordered and strong covalently bonded films on high-*k* oxide surfaces. Moreover, SAMs do not subdue the high capacitances. A hybrid dielectric bilayer consisting of an ultrathin high-*k* material and an SAM layer still shows less defects and a high capacitance, allowing a low-voltage operation. This technology reduces the gate dielectric thickness down to 10 nm or less and can be incorporated with ultrathin flexible substrates, making OFETs promising for potential applications in flexible, textile, and stretchable electronics.

Although great advances have been achieved in the effective surface functionalization of oxide dielectric substrates with SAMs, this method is not suitable for polymer dielectric substrates typically used in flexible electronics because of the limited dangling bonds thereon. To solve this issue, very recently, Yokota et al.[28] reported the development of a new three-bladed, propeller-shaped organic molecule, triptycene (Figure 2b), which can self-assemble into a completely oriented 2D hexagonal array and 1D multilayer stacking structure (Figure 2c).[27] Such few-layer modifying films are similar to conventional SAMs, on inorganic dielectric substrates, where they passivate the polymer surface to provide better electrical performance (Figure 2d). There is still a lot of room to develop efficacious surface modification methodologies to optimize the surfaces on flexible substrates and thus improve device performance.

3. Binary Interfaces in Functional Devices

OFETs are becoming one of the most important and promising platforms for building functional devices. Carefully engineering the semiconducting layer as well as the interfaces existing in an OFET, i.e., the OSC/electrode and OSC/dielectric interfaces, with a binary structure has been an effective approach to enhance the optoelectronic performance. The binary interface engineering method also provides a practical option for realizing functional devices.

3.1. Bi(multi)component Organic Semiconducting Layers

In a conventional OFET structure, the active semiconducting layer is composed of small molecules or polymers, which generally have large π-conjugated planes on their backbones for hole or electron carriers to diffuse throughout the whole bulk via inter- and intramolecular π–π interactions. By simply adding another component to form a bi(multi)component composite at the molecular scale, other noncovalent interactions, such as charge transfer interactions and H-bonding, can be induced in OSC solids. There is no doubt that the introduction of a new component into the active organic semiconducting layer influences the resultant optoelectronic characteristics of the devices. Therefore, the binary component strategy offers researchers a powerful methodology to improve the intrinsic performance of optoelectronic devices. The thickness of the active channel ranges from a few to hundreds of nanometers, corresponding to monolayer FETs and traditional device architectures. In this section, we mainly focus on traditional OFET devices, in which the semiconducting channel can be regarded as a 3D bulk layer. The introduction of molecular additives and nanowires (NWs) or nanotubes into bulk OSCs can lead to 0D/3D and 1D/3D composites, respectively. Using 2D materials, such as graphene and transition metal dichalcogenides (TMDs) with just one atom thickness, in contact with OSCs, 2D/3D heterojunctions can be constructed. Similarly, by depositing two semiconductors one on top of the other, a 3D/3D heterojunction can be obtained (see **Figure 3**). A different form of 3D/3D heterojunction can be prepared by blending two different kinds of OSCs together.

For 0D/3D semiconductor composites, the most representative example is the doped OSC system. Doping is a valuable method to tune the electronic performance.[89–92] In this, low-cost, effective, and especially commercially available solution-processed dopants are highly desirable. Recently, different small molecule additives have been mixed into OSCs to act as dopants. An organic electron acceptor is deposited to achieve p-type doping, whereas an organic electron donor leads to n-type doping. Although the mechanisms of the doping effects are complicated,[24,89] in the most common situation, the charge carrier density in the bulk of OSCs can be modulated and optimized through the doping effect. The concentration of dopants is crucial. Moderate doping leads to a high performance with improved mobility and threshold voltage (V_{th}) values because doping increases the charge carrier density. However, at a high doping concentration, usually large OFF currents are induced in unipolar OSCs, degrading the device performance.[93–96] Recently, Hu et al.[97] reported the use of a low-cost effective amidine-type n-dopant, 1,8-diazabicyclo[5.4.0]undec-7-ene (DBU), to dope electron-rich OSCs. This doping worked well in both solar cells and FETs. With 0.1 wt% DBU doped-[6,6]-phenyl-C_{61}-butyric-acid methyl ester ($PC_{61}BM$) as the electron-transporting layer, the fill factor of a perovskite solar cell with the device structure of indium tin oxide/NiO_x/$CH_3NH_3PbI_3$/n-doped $PC_{61}BM$/Ag could be enhanced from 0.54 to 0.76, and the power conversion efficiency (PCE) obtained was over 16%, much better than that of the undoped device with a PCE of about 10%. In addition, after doping with 0.1 wt% DBU, the mobility of the $PC_{61}BM$ OFET with a BGTC configuration was increased by about tenfold to be 5.35×10^{-3} cm^2 V^{-1} s^{-1}. Panidi et al.[98]

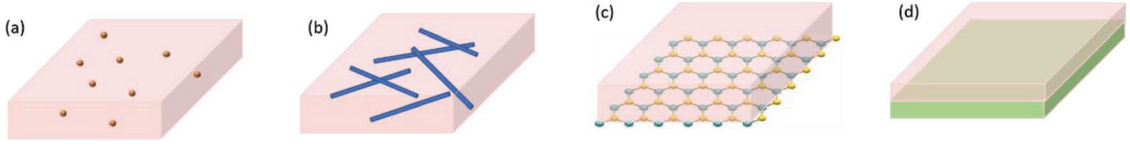

Figure 3. Illustration of bicomponent organic semiconducting layers. a) 0D/3D composite. b) 1D/3D composite. c) 2D/3D heterojunction. d) 3D/3D heterojunction.

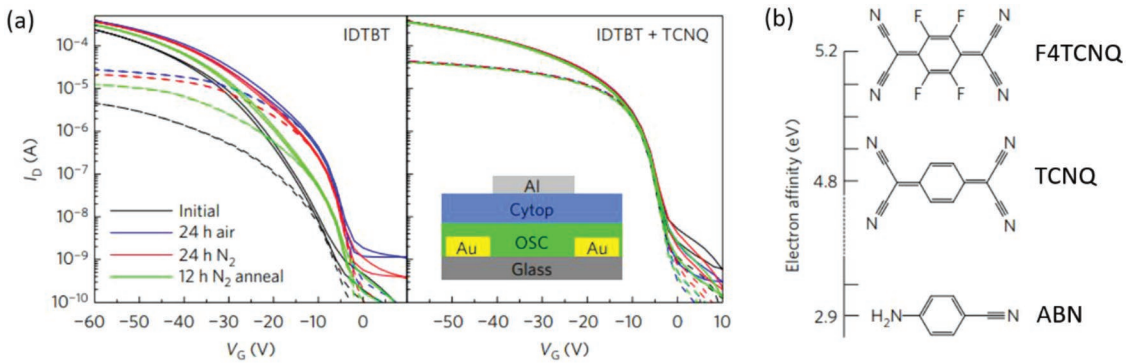

Figure 4. Improved polymer FET performance and the environmental/operational stability with molecular additives. a) Linear ($V_{DS} = -5$ V, dashed lines) and saturation ($V_{DS} = -50$ V, solid lines) transfer characteristics of IDTBT OFETs with (right) and without (left) 2 wt% of TCNQ additive. Measurements were taken successively for the as-prepared device, after 24 h exposure to first air and then nitrogen environments and after a 12 h anneal in nitrogen. b) Electron affinity of the F4TCNQ (top), TCNQ (middle), and ABN (bottom) additives. All panels reproduced with permission.[100] Copyright 2017, Nature Publishing Group.

reported that remarkable improvements in the hole mobility of p-type OSC systems could be realized by mixing with a molecular Lewis acid $B(C_6F_5)_3$. Strong interactions between the small molecule additives and OSCs were observed, and $B(C_6F_5)_3$ was considered to play a dual role, acting as an efficient p-type dopant and microstructure modifier. In addition, the influence of the doping effect on the electronic properties such as mobility, ON/OFF ratio, and V_{th} varies for different OSCs when using the same dopant because of their different electronic structures, e.g., the different levels of densities of states.[99]

By incorporating a common n-type dopant such as 4-aminobenzonitrile (ABN), tetracyanoquinodimethane (TCNQ), or tetrafluoro-tetracyanoquinodimethane (F4TCNQ) as a molecular additive into the active layer, Nikolka et al.[100] achieved a high operational and environmental stability of OFETs fabricated with films of p-type conjugated indacenodithiophene-*co*-benzothiadiazole copolymer (IDTBT) as channels (**Figure 4**). As shown in Figure 4a, the as-prepared pristine IDTBT OFET exhibited environmental instabilities with low ON currents and strong operation condition dependency. Even 2 wt% of the small molecule additive (like TCNQ) was sufficient to provide a near perfect environmental stability, and the FET with doped films showed a hysteresis-free electrical performance with very low shift in the V_{th}. The additive-induced improvement in stability was attributed to the removal of traps by the dopant, which might have reduced water's deleterious effects and prevented water from interacting directly with the polymers. Recently, Phan et al.[101] successfully improved the electrical stability and ideality by adding fullerene derivatives into a donor–acceptor (D–A) copolymer, poly[4-(4,4-dihexadecyl-4H-cyclopenta[1,2-b:5,4-b′]dithiophen-2-yl)-alt-[1,2,5]-thiadiazolo[3,4-c]pyridine]. The fullerene derivatives suppressed electron transport and electrical instability while maintaining a high hole mobility in the polymer-based FETs, changing the ambipolar OFETs to unipolar, with high ON/OFF ratios. To summarize, integration with doped organic thin films (0D/3D composites) as active channels can improve the electronic properties and environmental stabilities of organic devices.

CNTs, classical 1D materials, can form 1D/3D composites with conjugated polymer semiconductors. From a microscopic perspective, CNTs comprise rolled-up sheets of sp^2-hybridized carbon atoms wrapped into a cylindrical tube, having a large electron cloud density outside the wall, and capable of forming strong π–π interactions with aromatic molecules. Mixing CNTs with organic semiconducting polymers to act as an active layer can improve the carrier mobility of OFETs. It is not always easy to implement a homogenous dispersion of CNTs in the polymer matrix, due to the tendency of CNTs to form undesired aggregates via strong van der Waals interactions. But conjugated polymers with a similar aromatic structure could strongly interact with and well disperse SWCNTs. Therefore, some conjugated polymers have been used to sort SWCNTs for the proper separation of semiconducting CNTs.[103–105] Mixing small amounts of CNTs with semiconducting polymers could improve the injection of both holes and electron carriers in OFETs and is applicable for polymers with a wide variety of conjugated backbones.[106,107] Qu et al.[108] embedded SWCNTs in poly(9,9-dioctylfluorene-*co*-bithiophene) (F8T2) as the conduction channel to facilitate a systematic investigation of current hysteresis and showed different mechanisms for short-channel and long-channel devices. Moreover, incorporating functionalized double-walled CNTs into an OSC result in a good dispersion, thus leading to an enhancement in the OFET performance.[109,110] In addition, Yu et al.[102] reported the enhanced mobility of conjugated polymer OFETs mixed with multiwalled CNTs (**Figure 5**). With 1 wt% of undoped CNTs (U-CNTs) or boron-doped multiwalled CNTs (B-CNTs) added into the polymer films, the average mobilities were ≈0.012 $cm^2\ V^{-1}\ s^{-1}$ for a poly(3-hexylthiophene) (P3HT)/U-CNTs device and ≈0.044 $cm^2\ V^{-1}\ s^{-1}$ for a P3HT/B-CNTs device, i.e., sixfold and 23-fold higher than that of the pristine P3HT, and improved ON currents were obtained for both (Figure 5b). Particularly, the B-CNTs exhibited excellent dispersion mixing with polymers, even at a high concentration at which the U-CNTs formed undesired aggregation, and were capable of improving the mobilities in a wide range of concentrations (Figure 5c). The improved mobility of P3HT/B-CNTs was attributed to the significant reduction in activation energy and enhanced local crystallization. Moreover, taking advantage of the B-CNT technique,

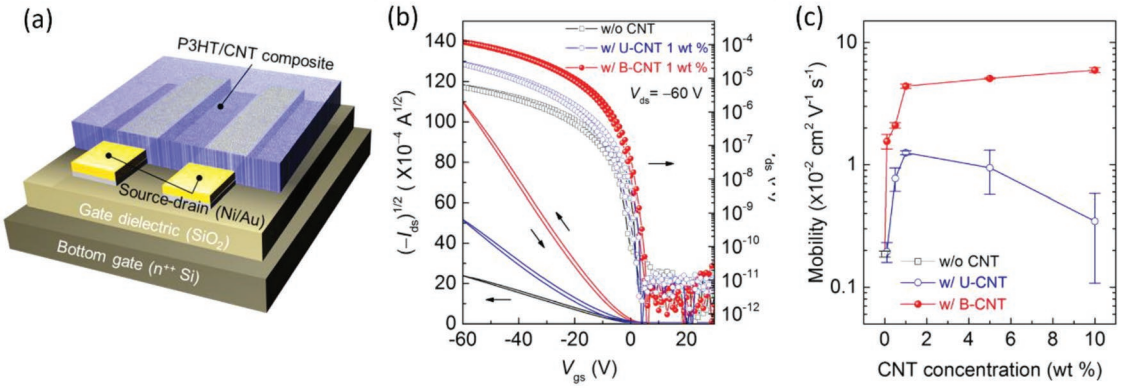

Figure 5. Device characteristics of P3HT/CNT OFETs. a) Cross-sectional diagram of the P3HT/CNT composite FET. b) Transfer characteristics of P3HT (with or without 1 wt % CNTs with respect to P3HT) FETs. c) Hole mobilities of P3HT/CNT composite FETs at various CNT concentrations. All panels reproduced with permission.[102] Copyright 2014, American Chemical Society.

the authors fabricated a flexible OFET on a plastic substrate consisting of B-CNT-mixed poly[2,5-bis(2-decyltetradecyl)-pyrrolo[3,4-c]pyrrole-1,4(2H,5H)-dione-alt-5,5′-di(thiophen-2-yl)-2,2′-(E)-2-(2-(thiophen-2-yl)vinyl)thiophene] (PDVT-10) and achieved high hole mobilities up to 7.2 cm^2 V^{-1} s^{-1} from ≈0.31 cm^2 V^{-1} s^{-1} of the pristine PDVT-10 film. In addition to the traditional 1D materials, CNTs, Hsieh et al.[111,112] reported the use of inorganic semiconducting NWs to form 1D/3D composites with OSCs. With nonpercolating silicon or germanium NWs added into polythiophenes as semiconducting layers, the OFET devices showed remarkable improvement in hole carrier mobilities and ON current, without any effect on the ON/OFF current ratios.

Since the isolation of graphene, the very first 2D material, in 2004, the concept of 2D materials has been well developed. From then on, a large number of 2D materials have been synthesized, such as 2D allotropes of elements, TMD monolayers, MXenes (2D transition metal carbides, carbonitrides, and nitrides), etc.[114–116] 2D materials possess sufficient electronic properties, with conductivity ranging from that of conductors to those of semiconductors and insulators, and offer additional choices for optoelectronic applications.[117,118] For example, graphene is an excellent conductor and can be used as a source/drain electrode. A variety of TMDs and black phosphorus are semiconducting materials and exhibit rather high mobilities. By combining semiconducting 2D materials, like TMDs, with OSCs, researchers can build 2D/3D heterojunctions to act as active components in the field of organic electronics.[119,120] Constructing heterostructures with p-type and n-type semiconductors is an efficient way to realize an ambipolar or antiambipolar operation in different types of devices, presenting potential advantages toward building organic circuits. In addition, heterojunctions are desirable for an efficient breaking of photoexcited excitons into free charge carriers for photoelectron conversion. Such well-defined heterostructures are usually applied for achieving high energy-conversion efficiency in organic photovoltaic devices. For example, a 2D/3D heterojunction composed of organic rubrene single crystals and 2D MoS_2 as the p- and n-type semiconductors, respectively, could exhibit diode-like good current-rectifying characteristics and gate-tunability, with a rectifying ratio up to 10^5, when applied in a three-terminal device (**Figure 6**a–d).[113] The p–n junction showed a high photoresponsivity of 510 mA W^{-1} under a light intensity of 20 mW cm^{-2}; a switch behavior with a fast response time (<5 ms) was also observed (Figure 6e).

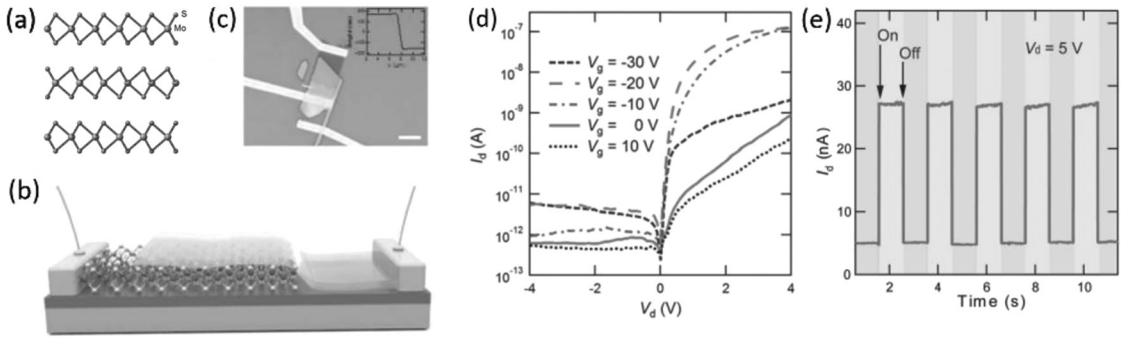

Figure 6. The 2D/3D heterojunction device based on MoS_2 and rubrene. a) The side view of the MoS_2 crystal structure. b) Top view and c) optical images of the p–n junction device that rubrene single crystal placed between the MoS_2 flake and the gold electrode. d) The I_d–V_d curve of the p–n junction under different gate voltage, showing typical rectifying behavior. e) The switch behavior of the p–n junction under the light illumination on and off alternatively. All panels reproduced with permission.[113] Copyright 2015, Wiley-VCH.

High-performance photoresponsive FETs could also be built using a 2D/3D MoS_2/pentacene heterojunction.[121] In another work, He et al.[122] successfully fabricated an ambipolar OFET using the heterojunction of a MoS_2/rubrene heterostructure as the channel layer, which could show hole and electron mobilities of ≈0.36 and ≈1.27 $cm^2\ V^{-1}\ s^{-1}$, respectively. In addition, the 2D/3D heterojunction can also function to yield antiambipolar behaviors, which means that the current can only transport across the channel in a specific range of gate voltage under source–drain biases. Asymmetric antiambipolar transfer curves with different transconductances were observed for the three-terminal devices based on MoS_2/pentacene heterojunctions.[123] Upon illumination, a clear photovoltaic effect was observed from the devices, with an open circuit voltage (V_{OC}) ≈0.3 V and a short circuit current (I_{SC}) ≈ 3 nA. Yu et al.[124] demonstrated hybrid heterojunctions based on semiconducting TMDs, MoS_2 or $MoSe_2$, with a functionalized perylene-diimide as the OSC, at which efficient charge separation and improved photon harvesting could be realized.

Integrating p- and n-type OSCs layer-by-layer can result in a 3D/3D structure, i.e., OSC/OSC heterojunction, which could be used to achieve ambipolar charge transport and photoinduced charge separation, similar to the case of 2D/3D structures. Both small molecules and conjugated polymers have been applied to build 3D/3D heterojunctions. With the capability of combining the optoelectronic properties of single components together, the idea of fabricating organic heterojunctions provides an approach for functional organic devices.[127] Moreover, taking advantage of alignment and patterning of the OSC, a crystalline heterojunction could be fabricated, facilitating a broad insight into organic materials and the development of various optoelectronic devices.[128–131] For example, ambipolar charge transport was obtained from an organic single-crystalline heterojunction of C_8-BTBT ribbon crystals as the p-type and C_{60} needle crystals as the n-type material, which showed a best performance of ≈0.16 $cm^2\ V^{-1}\ s^{-1}$ for hole mobility and ≈0.17 $cm^2\ V^{-1}\ s^{-1}$ for electron mobility.[132] Fabricated on plastic substrates with a polymer dielectric layer, flexible ambipolar OFETs could be realized using vacuum-deposited OSC p–n heterojunctions.[133] Very recently, Zhang et al.[125] developed a surface-energy-controlled stepwise crystallization method for the preparation of organic heterojunctions. They successfully obtained laterally stacked heterojunction arrays composed of a single-crystalline microbelt (MB) of p-type 2,8-difluoro-5,11-bis(triethylsilylethynyl) anthradithiophene (dif-TES-ADT) and n-type *N,N*-bis(2-phenylethyl)-perylene-3,4:9,10-tetracarboxylic diimide (BPE-PTCDI), which could exhibit balanced ambipolar transport, with hole and electron mobilities of 0.32 and 0.43 $cm^2\ V^{-1}\ s^{-1}$, respectively (**Figure 7**a–c). Yao et al.[126] developed a novel method to build high-performance organic optoelectronic devices by directly photolithographing molecular crystals. Through this method, they built heterojunction devices based on n-channel *N,N′*-dioctyl-3,4,9,10-perylenedicarboximide (PTCDI-C8) NWs and p-channel 2,7-diphenyl[1]benzothieno[3,2-b][1]benzothiophene (Dph-BTBT) nanoflakes, using asymmetric Au–Ag electrodes. The device exhibited a photovoltaic effect through which the V_{oc} could be significantly improved under illumination, with an increase in the wavelength of light (Figure 7d,e). In addition, Kobashi et al.[134] reported the development of an organic antiambipolar transistor (AAT) with a bottom-gate configuration, based on a heterojunction consisting of α-sexithiophene (α-6T) and PTCDI-C8. In a subsequent study, they[135] constructed a ternary inverter consisting of an organic AAT and an n-type OFET, which could be used as a three-distinct-logic device with a low operating voltage below 10 V. Apart from the heterojunctions built with OSC components, Wu et al.[136] reported a heterojunction based on ferroelectric single crystals of $CdCl_3$ grown on top of well-aligned C_{60}, which could be used to fabricate FET-based memory devices. With the ferroelectric/semiconductor bilayer heterojunction as the channel layer, a large memory window with a long retention time was realized. Equally importantly, the electron mobilities of the bilayer devices were as high as that of C_{60} single-crystal devices. In addition to the small molecule-based OSC heterojunctions, conjugated polymers have also been applied to construct bilayer heterojunctions. Recently, She et al.[137] reported a vertical organic transistor for fast nonvolatile memory, incorporating a unipolar p-type small molecule, pentacene, on top of an ambipolar conjugated polymer, poly(*N*-alkyl-diketopyrrolo-pyrrole dithienylthieno [3,2-b] thiophene) (DPP-DTT), which could be operated within 150 ns for programming and 50 ns for erasing, respectively. Kim et al.[138] reported the preparation of an all-polymeric bilayer heterojunction using p-type and n-type conjugated polymers with matched energy levels, PDVT-10 and poly[[*N,N′*-bis(2-octyldodecyl)-naphthalene-1,4,5,8-bis(dicarboximide)-2,6-diyl]-alt-5,5′-(2,2′-bithiophene)] (P(NDI2OD-T2), which enabled highly balanced ambipolar charge transport properties with hole and electron mobilities of 0.32 (±0.05) and 0.25 (±0.02) $cm^2\ V^{-1}\ s^{-1}$, respectively, in a top-gate bottom-contact (TGBC) FET.

In addition, by blending two p-type OSCs together, an improved device performance can be obtained from transistors.[139,140] For example, using a blend of a small molecule and polymer (2,7-dioctyl[1]-benzothieno[3,2-b][1]benzothiophene (C_8-BTBT) and indacenodithiophene-benzothiadiazole (C_{16}IDT-BT), respectively), the resulting TGBC OFETs could exhibit maximum a hole mobility of ≈4.7 $cm^2\ V^{-1}\ s^{-1}$, an improved value in comparison with that of controlled devices made of a single component (*viz.*, C_8-BTBT ≈2.6 $cm^2\ V^{-1}\ s^{-1}$ and C_{16}IDT-BT ≈3.1 $cm^2\ V^{-1}\ s^{-1}$). Moreover, by introducing a p-dopant, 1% mol $C_{60}F_{48}$, into the blend, the performance could be dramatically enhanced, leading to a maximum hole mobility exceeding 13 $cm^2\ V^{-1}\ s^{-1}$. Furthermore, by introducing photochromic molecules into the organic semiconducting layer in an OFET, the resulting functional device can be switched by light under different wavelengths. Leydecker et al.[141] reported the use of an organic bicomponent blend of a polymer semiconductor P3HT and a photochromic diarylethene (DAE) to build flexible nonvolatile optical memory organic transistors, capable of being switched with 3 ns laser pulses. The three-terminal devices could be integrated to create high-density robust memories with 8 bit memory units that could endure over 70 write–erase cycles and show a retention time of over 500 d.

3.2. Binary Contact Modification

An efficient charge injection process from the source electrode (mostly metal) to the channel is one of the critical issues

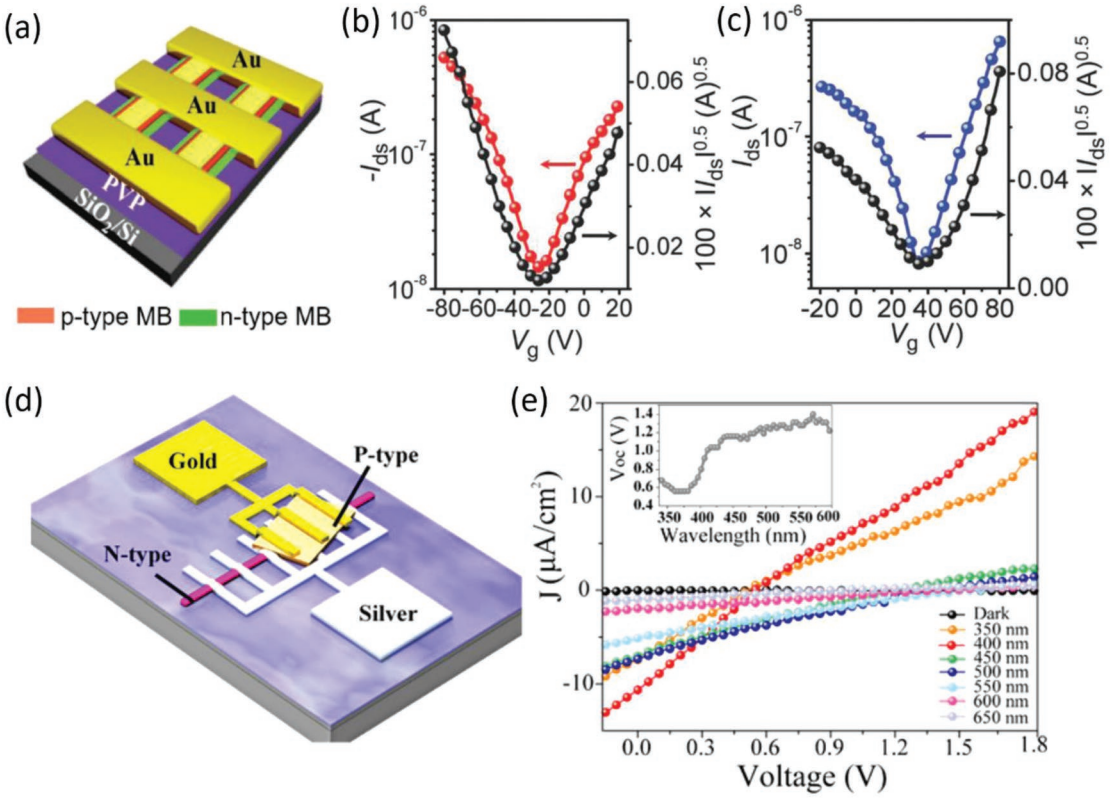

Figure 7. Organic 3D/3D heterojunction devices. a) Schematic device diagram of the ambipolar OFETs based on p–n junction MB arrays. Typical transfer characteristics of the OFET b) in p-channel operation mode under negative drain bias and c) in n-channel operation mode under positive drain bias. d) 3D schematic diagram of the D–A heterojunction photovoltaic device based on PTCDI-C8 NWs and Dph-BTBT nanoflakes. e) *J*–*V* curves in the dark and upon illumination at different wavelengths and the inset showing the V_{oc} significantly increases from 0.56 to 1.4 V with the illumination wavelength changing from 320 to 690 nm. (a–c) Reproduced with permission.[125] Copyright 2018, Wiley-VCH. (d,e) Reproduced with permission.[126] Copyright 2018, American Chemical Society.

to realize high-performance organic optoelectronic devices. If not satisfied, the contact resistance will be very high, resulting in poor electronic characteristics. In other words, an Ohmic contact is always desired to realize the maximum current density. To optimize the charge injection properties at the OSC/electrode interface, several efficient strategies have been developed to reduce the contact resistance, such as modifying the metal electrode with SAMs and introducing interlayers of metal oxides/metal salts or organic compounds into the metal–organic interface.[1]

As discussed in Section 2, SAMs have been widely utilized to modify a variety of metals, as a kind of nanotechnology.[144] Recently, Alt et al.[142] used a novel bisjulolidyldisulfide (Juls) SAM (**Figure 8**a) to modify Au or Ag electrodes; it was capable of lowering the work functions of the electrodes by ≈1.2 eV, thus resulting in to a proper match with the lowest unoccupied molecular orbital (LUMO) of n-type OSCs. Using the Juls SAM to treat the source/drain electrodes in N2200-based OFETs could significantly facilitate electron injection into the channels (Figure 8b,c). As shown in Figure 8c, a two orders of magnitude reduction in the contact resistance, in comparison with that of the pristine ones, occurred. Huang et al.[145] reported high-speed UV phototransistors based on $PC_{61}BM$, with ambipolar transport. They chose pentafluorothiophenol (PFBT) to modify Au electrodes, and balanced p- and n-type transport characteristics were obtained in the dark, with electron and hole mobility values of 0.14 and 0.06 $cm^2\ V^{-1}\ s^{-1}$, respectively. In addition, recent studies have shown that the improvement in the contact between SAM-modified metal electrodes and OSCs is not only because of the work function tuning of metals by the SAM-induced surface dipole, and that SAMs can influence the nucleation behaviors of the organic molecules on top of them.[26,146,147] Niazi et al.[147] investigated the influence of chemical modifications of Au bottom electrodes on the contact with different small-molecule OSCs in bottom-gate bottom-contact (BGBC) FETs. They used several fluorinated phenylthiols to modify Au electrodes and then deposited OSCs or their blends with an insulating polymer, on them, by spin-coating and blade-coating processes. A desirable contact-induced nucleation occurred when they were deposited by spin coating, resulting in high-performance OFETs with mobilities ranging 3–5 $cm^2\ V^{-1}\ s^{-1}$.

Moreover, if an SAM molecule contains a photochromic group, its dipole can be changed under illumination, and it can be used for building photoactive devices.[143,148] For example, Zhang et al.[143] developed an optically switchable OFET by integrating a photochromic spirothiopyran (SP) SAM-functionalized semiconductor/electrode interface (Figure 8d). The open and closed forms of SP affected the charge injection barrier of

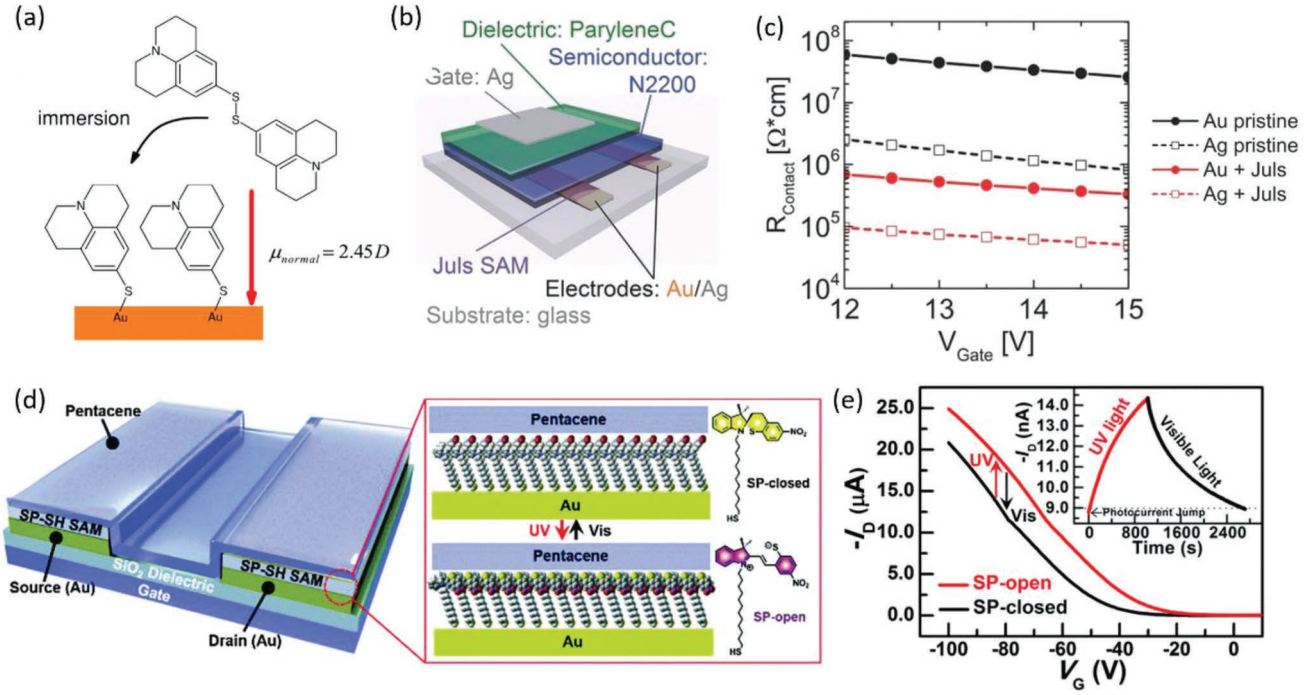

Figure 8. SAM modification of electrodes in OFETs. a) Molecular structure of Juls and surface-accumulated configuration. b) Illustration of the OFET stack. c) Contact resistances of OFETs with pristine and Juls-treated Au and Ag electrodes, determined with the transfer line method (TLM). d). Schematic illustration of the OFET with Au electrodes modified by SP SAMs. Photochromic SP molecules can undergo reversible photoisomerization between closed and open states. e) Transfer properties of a device before and after UV irradiation. (a–c) Reproduced with permission.[142] Copyright 2016, Wiley-VCH. (d,e) Reproduced with permission.[143] Copyright 2014, Royal Society of Chemistry.

holes into the pentacene channel layer; hence, the contact resistance varied, leading to a high and low current level under UV illumination and under visible light, respectively (Figure 8e).

Inserting suitable thin interlayers into the metal/organic interface could facilitate carrier injection and reduce the interface contact resistance. A variety of materials have been proven effective as interlayers to enhance device performance in the field of organic electronics, as mentioned in Section 2. For example, Gang et al.[32] reported a new low-temperature atomic layer deposition process (ALD) of V_2O_5, for organic devices, without degrading the delicate OSCs (**Figure 9**a). With a high-quality VO_x interlayer to enhance the hole injection, the authors observed an improvement in the electronic performance of p-type OFETs based on pentacene, using different metals (Au or Cu) as electrodes. The authors found that the Cu/VO_x/pentacene OFET device with 40 ALD cycles of VO_x exhibited the best performance, with the mobility enhanced to 0.80 $cm^2\ V^{-1}\ s^{-1}$ (compared with 0.29 $cm^2\ V^{-1}\ s^{-1}$ for the untreated condition and 0.54 $cm^2\ V^{-1}\ s^{-1}$ for the 80 ALD cycles condition), which was attributed to the tradeoff between the fine-tuning work function and highly resistive nature of VO_x (Figure 9b). Baeg et al.[35] reported that inserting a thin layer of a cesium (Cs) salt, Cs_2CO_3 or CsF, could tune the electrode work function, significantly enhancing the electron injection in ambipolar OFETs, at the Au/OSC (different conjugated polymers were used) interface, with only a slight degradation in the p-channel performance. The effectiveness of organic molecules used as interlayers at the semiconductor/electrode interface to control the work functions and improve the electrical performance has also been highlighted. Recently, Kanagasekaran et al.[149] demonstrated a new electrode-modifying strategy, using a bilayer of tetratetracontane (TTC) and polycrystalline OSCs (pc-OSC) to cover the metal electrodes (Figure 9c). When the asymmetric electrodes, Ca/pc-OSC/TTC and Au/pc-OSC/TTC, were employed for electron and hole injection in rubrene-based OFETs, the mobilities of holes and electrons were ≈22 and ≈5.0 $cm^2\ V^{-1}\ s^{-1}$, respectively, which are among the highest two-terminal field-effect mobilities reported for the corresponding semiconductors (Figure 9d).

In addition, doped polymers could influence the charge injection process when used as metal-surface modifiers. Tang et al.[150] reported that by using self-assembled interlayers made of highly doped semiconducting polymers, with ultrahigh or ultralow work functions, at the organic/electrode interfaces, the work function could be tuned to be ultrahigh or ultralow, suitable for Ohmic contacts in organic devices such as OLEDs, OFETs, and organic solar cells. With different conjugated backbones, self-compensated hole-doped triarylamine-fluorene copolymers can provide work functions as high as 5.8 eV, whereas self-compensated electron-doped naphthalene-bis(carboxyimide)-thiophene copolymers are capable of showing low work functions down to 3.9 eV. When using doped polymers to modify Au electrodes, the ambipolar behaviors of a D–A conjugated polymer, poly(2,5-bis(alkyl)-1,4-dioxopyrrolo[3,4-c]pyrrole-3,6-diyl-thiophene-2,5-diylthieno[2,3-b]thiophene-2,5-diyl-thiophene-2,5-diyl) (DPPT2-T), could be transformed into those of p- or n-FETs, alternatively (Figure 9e,f). Seah et al.[151] used a polyelectrolyte counterion monolayer as the

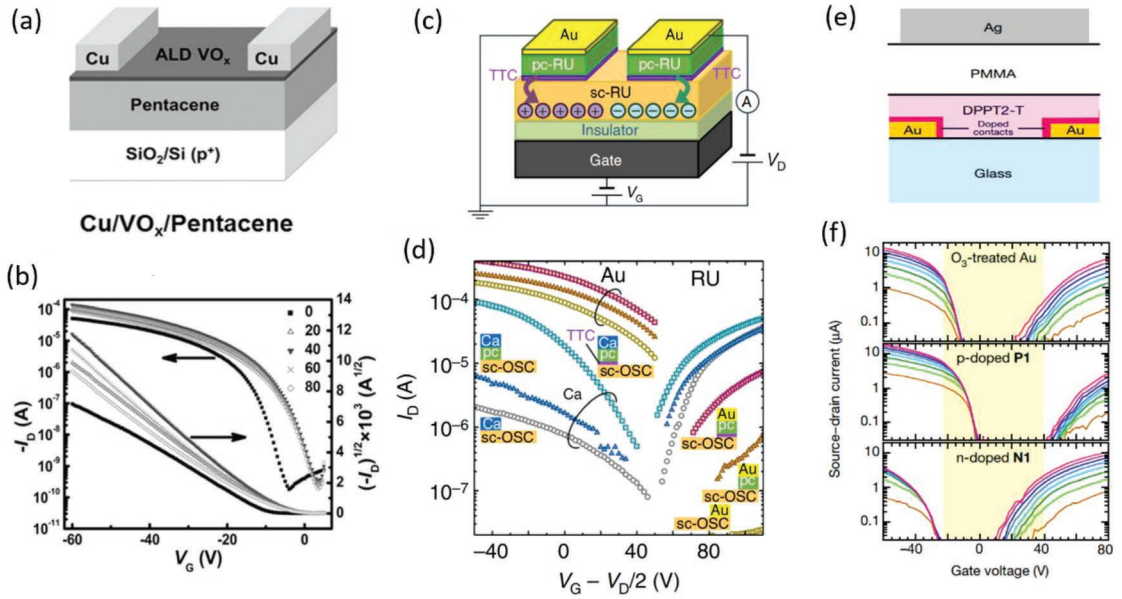

Figure 9. Electrode modification with interlayer. a) Schematic illustration showing the BGTC structure of the Cu/VO_x/pentacene OFET device. b) Comparison of the associated transfer characteristics without and with VO_x of different ALD cycles. c) Schematic illustration of a rubrene single crystal FET with electrodes modified with a pc-OSC/TTC layer. d) Transfer characteristics of rubrene OFETs with various electrodes, respectively. e) Schematic of the DPPT2-T OFET structure with self-aligned assembly of ultrahigh- or ultralow-work-function interlayers. f) Transfer characteristics of the device with a monolayer of p-doped P1 (middle) or n-doped N1 (bottom). (a,b) Reproduced with permission.[32] Copyright 2016, Wiley-VCH. (c,d) Reproduced with permission.[149] Copyright 2017, Nature Publishing Group. (e,f) Reproduced with permission.[150] Copyright 2016, Nature Publishing Group.

interlayer to dope the contact interface and achieved Ohmic contacts with contact resistivities in the range of 0.1–1 Ω cm^2. With a self-aligned polyelectrolyte counterion interlayer, an enhancement in performance could be realized for both p- and n-type OFETs.

The use of carbon-based materials such as graphene, as electrodes in direct contact with OSCs, is another promising method to enhance charge injection.[154,155] As early as 2009, Cao et al.[152] reported the use of SLG in contact with thin films of P3HT to realize high-performance OFET devices (**Figure 10**a). A high ON/OFF ratio and bulk-like hole carrier mobilities of ≈1.4 × 10^{-3} cm^2 V^{-1} s^{-1} were obtained in a lateral geometry FET, as shown in Figure 10b. In fact, graphene electrodes can be integrated with OSCs for both lateral and vertical device architectures to overcome the performance limitations of metal electrodes.[155] Recently, Sun et al.[153] built vertical OFETs (VOFETs) using graphene as source electrodes and thin films of 2D covalent organic frameworks (2D COFs), constructed by employing 1,3,6,8-tetrakis(*p*-formylphenyl)pyrene (TFPy) and *p*-phenylenediamine (PPDA), as the semiconducting channel, which showed an ambipolar transport behavior under a low modulating voltage (Figure 10c,d). The suitable injection barrier at the graphene/COF interface led to a high ON/OFF ratio and high ON current density. Better electronic characteristics can be also realized using surface-modified graphene electrodes, as reported by Kang et al.[156] Octadecyltrimethoxysilane (ODTS) could assemble onto the surface of graphene by weak epitaxial assembly. The authors found that the OFETs with ODTS-modified graphene (denoted as ODTS-G) showed higher hole mobility values and ON/OFF ratios.[156] As the ODTS modification also increased the mechanical durability, they further demonstrated an ultrathin flexible OFET array using ODTS-G as the source, drain, and gate electrodes, which worked well and showed only a slight degradation under mild crumpling. In addition, reduced graphene oxide (rGO) can also be used as electrodes, suitable for both electron and hole injections (**Table 1**).[157,158]

3.3. Responsive Dielectric Layers in Functional OFETs

The accumulated mobile carriers in the active channel of an OFET are induced at the OSC/dielectric interface by an applied gate voltage (higher than V_{th}), which is proportional to the capacitance of the dielectric layer as well. Then, under the source/drain bias, the current comes out along the channel, i.e., by changing the properties of the organic/dielectric interface or the dielectric layer, the device performance can be fine-tuned. Integrating responsive materials at the interface provides a practical method for fabricating functional OFET devices that are responsive to light, pressure, magnetic force, etc.[174,175]

By focusing on the functionalization at the OSC/dielectric interface, Zhang et al.[178] used a functional SAM bearing a photochromic spiropyran group (SP-SAM) to control the interfacial properties in a pentacene-based OFET. The photoisomerization of SP-SAM led to a change in the interfacial dipoles and produced two distinct built-in electric fields at the OSC/dielectric interface, which resulted in the modulation of the channel conductance and consequently, the V_{th}. Therefore, the interface-functionalized OFETs could function as a noninvasive memory device. Recently, Chen et al.[81] also reported a high-performance nonvolatile organic memory transistor featuring a photoactive

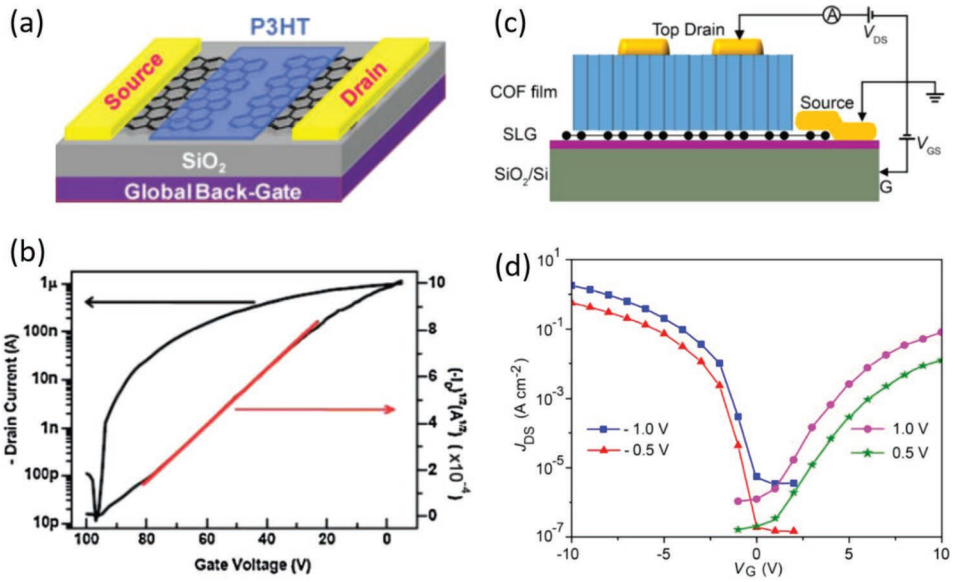

Figure 10. Graphene as contact electrodes in lateral and vertical OFETs. a) Device structure of P3HT lateral transistors with graphene as source/drain electrodes. b) Transfer characteristics for the device. c) Side view of the constructed COF/SLG-VOFET device. d) Transfer characteristics of the ambipolar COF transistor. (a,b) Reproduced with permission.[152] Copyright 2009, Wiley-VCH. (c,d) Reproduced with permission.[153] Copyright 2017, American Chemical Society.

hybrid bilayer dielectric (**Figure 11**a,b). A high-*k* HfO*x* dielectric layer was used to enable a low operation voltage of −3 V. A SAM of photochromic DAEs could undergo photoisomerization under illumination by lights of different wavelengths. The transistors could be programmed by light signals and erased by electrical signals, thus behaving as memory devices with long retention times and excellent reversibility.

A pressure sensor is another typical application that takes full advantage of a semiconductor/dielectric interface. Mannsfeld et al.[176] used microstructured elastomer polydimethylsiloxane (PDMS) films as the gate insulator and single-crystalline rubrene as the semiconducting channel to build highly sensitive flexible pressure sensors (Figure 11c–e). Under additional pressure, the shape of the microstructured PDMS films changed, i.e., the capacity of the insulator would change simultaneously, thus influencing the channel current. Recently, the development of flexible pressure sensors has attracted much research interest because of its diverse promising applications in smart wearable devices for wearable electronics, health monitoring, as well as electronic skin applications. Zang et al.[177] presented flexible suspended gate OFETs (SGOFETs) for ultrasensitive pressure detection (Figure 11f–h). The key point is the air gap space, which could change with the applied pressure. The capacity of the air dielectric layer was changed when its thickness decreased under pressure. With the suspended gate geometry, fine-tuning of the sensitivity could be achieved by altering the protective dielectric layer. Both an ultrahigh sensitivity (≈192 kPa^{-1}) and fast response (<10 ms) were realized in the SGOFETs. Based on the SGOFET concept, Zang et al.[179] proposed magnetic sensors where the gate electrode could deform under a magnetic force. AgNWs/Fe_3O_4/PDMS composites were chosen as the suspended electrodes, with excellent conductivity (Ag) and fine-tuned magnetic properties (Fe_3O_4). The devices showed a very high sensitivity of ≈115.2% mT^{-1} and could detect magnetic fields as low as ≈500 µT. These functional responsive dielectrics greatly enriched the functionalization strategy of the OFET. However, several fundamental issues, such as how to achieve multifunctionality, and balance between performance and functionality, call for more thinking and input.

As the charge transport behaviors within the channel layer are sensitive to external stimuli, this allows the corresponding OFET to work as a platform for gas sensors when exposed to an external environment because the gas molecules are capable of diffusing into the channel near the OSC/dielectric interface and affecting the charge transport behaviors.[182,183]

In principle, the most direct method toward maximum sensitivity is to use the "buried" conductive channel as the direct interaction interface, i.e., to make analyte molecules directly adsorb onto the conductive channel without diffusion through a dense semiconductor film. Shaymurat et al.[180] utilized an OFET with an air dielectric layer to address this requirement. An improvement in the sensitivity for sulfur dioxide (SO_2) detection was observed thanks to the enhanced interaction. The air dielectric-based device exhibited a high sensitivity of 119% for a low detection limit of 500 ppb (**Figure 12**a–c). In addition, the exposure of the first few layers in the active channels at the dielectric/semiconductor interfaces offers a direct interaction between the conductive channel and the analyte, resulting in an improvement in the sensitivity and response speed. For example, Zhang et al.[184] employed n-type naphthalene diimide derivatives (NDIs) to construct ultrathin-film devices. In contrast to conventional OFETs, the devices with an ultrathin active layer exhibited a faster response and higher sensitivity toward the analytes. The response signal of such ultrathin devices to 100 ppm ammonia (NH_3) was one order of magnitude stronger than that of a thick-film (70 nm)

Table 1. Summary of contact modification in OFETs (extracted from the literature published in recent three years).

Source/drain electrode		Modification	OSC	Device structure	Mobility [$cm^2 V^{-1} s^{-1}$]	Reference
SAM/metal	Au	PFBT	P3HT	BGBC	0.055 (h)	[159]
	Au	PF2BT	P3HT	BGBC	0.040 (h)	[159]
	Au	PF2BT	IIDDT-C3	BGBC	0.14 (h)	[159]
	Au	TFMBT	Pentacene	BGBC	0.086 (h)	[58]
	Au	PFBT	TIPS-pentacene/PTAA	TGBC	0.7 (h)	[160]
	Au	PFBT	$PC_{61}BM$	TGBC	0.14 (e)	[145]
	Au	PFBT	diF-TES-ADT:PαMS	BGBC	3.6 (h)	[147]
	Au	PFBT	TIPS-pentacene:PαMS	BGBC	4.6 (h)	[147]
	Au	DAE-SAM	P(NDI2OD-T2)	TGBC	0.17 (e)	[148]
	Au	BP0-down	pentacene	BGBC	0.2 (h)	[161]
	Au	BP0-up	C_{60}	BGBC	0.23 (e)	[161]
	Au	IPr	Pentacene	BGBC	0.15 (h)	[58]
	Ag	TP	P(NDI2OD-T2)	TGBC	0.11 (e)	[162]
	Ag	JuIs	P(NDI2OD-T2)	TGBC	0.1 (e)	[142]
Interlayer/metal	Au	$Mo(tfd)_3$	TIPS-pentacene/PTAA	TGBC	0.8 (h)	[163]
	Au	MoO_3	TIPS-pentacene/PTAA	TGBC	0.6 (h)	[163]
	Au	MoO_x	Pentacene	BGBC	0.15 (h)	[164]
	Au	VO_x	BOPAnt	BGTC	1.56 (h)	[32]
	Au	VO_x	Pentacene	BGTC	2.3 (h)	[165]
	Au	F6-TCNNQ	Pentacene	BGTC	0.1 (h)	[166]
	Au	Polyelectrolyte counterion	DPPT2-T	TGBC	0.2 (h)	[151]
	Au	pc-OSC/TTC	Rubrene	BGTC	22.0 (h)	[149]
	Ag	TPD	Pentacene	BGTC	0.1 (h)	[167]
	Al	MO_x	Styrylbenzene	BGTC	0.32 (h)	[168]
	Cu	VO_x	Pentacene	BGTC	0.87 (h)	[32]
	Cu	CuI	Pentacene	BGTC	1.27 (h)	[169]
	Cu	CuTCNQ	H-Ant	BGBC	0.64 (h)	[170]
	Cu	TPD	Pentacene	BGTC	0.11 (h)	[167]
	Ca	pc-OSC/TTC	Rubrene	BGTC	5.0 (e)	[149]
	Mo	MoO_3	DPPT-TT	TGBC	1.85 (h)	[171]
Carbon material	Graphene		P(NDI2OD-T2)	BGBC	0.0106 (h)	[155]
			P(NDI2OD-T2)	VOFET	–	[155]
			$COF_{TFPy\text{-}PPDA}$	VOFET	–	[172]
			pDTTDPP-DT	BGBC	1.38 (h)/2.82 (e)	[173]
		ODTS	DNTT	BGBC	0.79 (h)	[156]
		ODTS	Pentacene	BGBC	0.14 (h)	[156]
		ODTS	C_8-BTBT	BGBC	0.12 (h)	[156]
	rGO		PTCDI-C8	VOFET	–	[158]

device. Recently, Huang et al.[181] reported a highly sensitive OFET-based NO_2 sensor using a simple and low-cost UV-ozone (UVO) interfacial modification. The polymeric dielectric consisted of a layer-by-layer structure of polystyrene (PS) and poly(vinyl alcohol), of which the former was in contacted with a CuPc channel layer. After UVO-treatment with the PS interface, an enhancement of 400 × greater NO_2 sensitivity was obtained, compared with that of the untreated device, with a lower limit of detection (LOD) of ≈400 ppb. The authors attributed the high sensitivity to the oxygen-containing groups introduced by UVO treatment on the dielectric interface, which could strongly interact with NO_2 via physical adsorption, resulting in the formation of mobile positive charge carriers (Figure 12d–f). Wang et al.[185] realized ultrahigh-performance OFET-based NO_2 sensors with crystalline 6,13-bis(triisopropylsilylethynyl)pentacene (TIPS-pentacene)/*p*-6P films as active heterojunction channels, showing a short response/recovery time (within 200/400 s) with an extremely low LOD of 20 ppb. The authors revealed that the ultrasensitivity

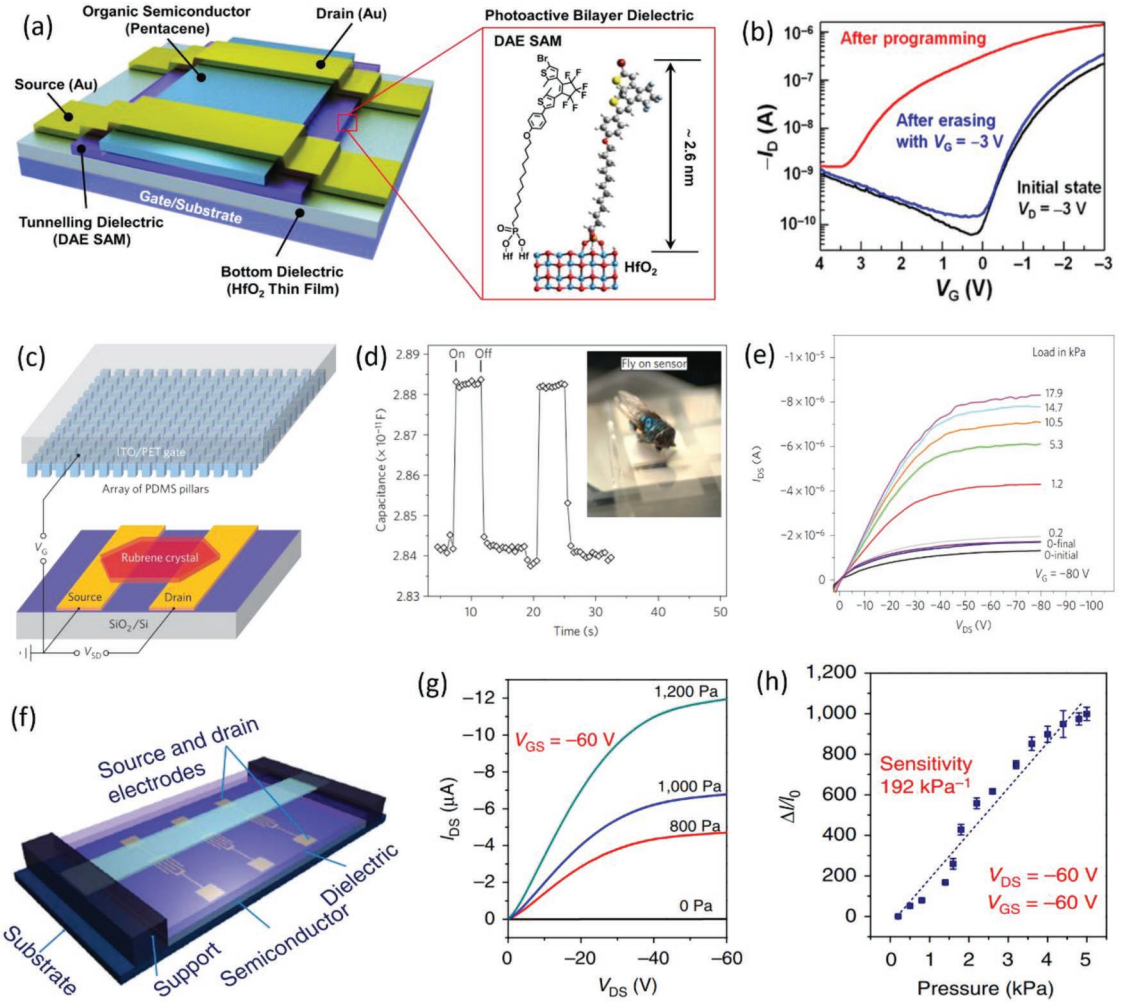

Figure 11. Stimuli-responsive dielectrics. a) Schematic cross-section of an organic memory transistor based on a photoactive hybrid bilayer dielectric. The inset shows the molecular structure and a real-space model of a DAE bonding to the HfO_2 surface. b) Large V_T window when V_G scanned from −3 to 4 V; V_D = −3 V. c) Schematic diagram of pressure-sensing OFETs, consisting of thin rubrene single crystals and structured PDMS dielectric films. d) The microstructured PDMS films are able to sense the application of very small pressures (even the moving of fly, corresponding to a pressure of only 3 Pa). e) Output curves of a transistor-based sensor with different external pressures applied. f) Schematic diagram of an SGOFET-based pressure sensor. g) Output curves of an SGOFET sensor taken at different applied pressures. h). Pressure response of the source–drain current at constant voltage V_{DS} = −60 V and V_{GS} = −60 V. (a,b) Reproduced with permission.[81] Copyright 2016, American Chemical Society. (c–e) Reproduced with permission.[176] Copyright 2010, Nature Publishing Group. (f–h) Reproduced with permission.[177] Copyright 2015, Nature Publishing Group.

(to NO_2 of more than 1000% ppm^{-1} at several ppm) is strongly related to the film charge transport ability, and finally pointed out the important impact of the charge transport of the semiconducting molecules on the sensor performance, i.e., a combination of high mobility and low initial carrier concentration is the key to realize the ultrasensitive sensors for oxidizing gases, such as NO_2.

4. Ternary Interfaces in Hybrid Devices

One of the key requirements in the fields of micro- and nanoelectronics is the use of external stimuli to modulate the functions of optoelectronic devices. Through this, a large number of potential applications such as sensing, detecting, and switching can be realized. FETs, applying organic materials as well as low-dimensional nanomaterials, such as Si NWs, SWCNTs, and graphene as conductive nanomaterials, have provided ideal platforms for sensing applications.[182] However, the traditional sensing mechanism of FETs has been restricted to analyte diffusion into the semiconductor surfaces which may cause serious problems in device stability, reversibility, and sensitivity because of the weak interaction between the physically adsorbed analytes and the semiconductors. As a result, the integration of active semiconducting materials, with stimuli-responsive components, into functional devices is important. Herein, we raise the term "ternary interfaces" (Figure 1e), such as semiconductor/recognition receptor/environment ternary interfaces, for specific physical/chemical/biosensing, or dye/SLG/TiO_2 ternary interfaces, for efficient charge transport and photovoltaic conversion. This method to modify semiconductor/environment interfaces has been proven efficient to

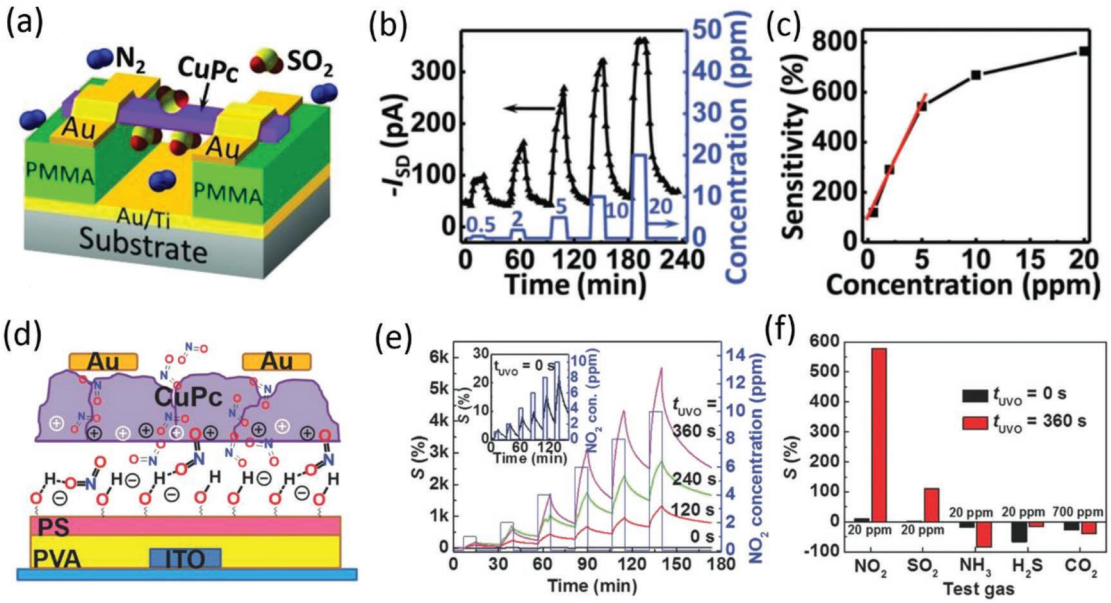

Figure 12. OFET-based gas sensors. a) Schematic of gas dielectric OFETs based on CuPc NWs. b) Real-time I_{SD} change of device to various SO_2 concentration (0.5, 2, 5, 10, and 20 ppm) at room temperature. The blue line corresponds to SO_2 concentration (right y-axis). c) Sensitivity of a device as a function of SO_2 concentration with the red line is the linear fitting result in low concentration SO_2. d) Schematic representations of the OFET-based NO_2 detectors showing the sensing mechanism. e) Real-time sensitivity responding to dynamic switching between NO_2 concentrations. f) Sensitivities of sensors with both UVO-untreated and treated for different gas species. (a–c) Reproduced with permission.[180] Copyright 2013, Wiley-VCH. (d–f) Reproduced with permission.[181] Copyright 2017, Wiley-VCH.

build novel nanoscale devices with desired functionalities that are capable of potential applications in functional devices. The key to this idea is to separate the signal recognition from charge transport, each performing its own function without interfering with the other.

4.1. Modified Interfaces in 1D Structures

Initially, our group used PDMS stamps (**Figure 13**a) to attach an alkane-containing spiropyran layer onto the surface of pentacene films, without destroying the FET. It was shown to efficiently and reversibly modulate the conductivity of FETs in a noninvasive manner.[3] However, the electrical conductivity of the photochromic spiropyran-coated surface decreased after several switching cycles. To improve the photoswitching stability of devices, we used different photoactive nanomaterials, such as nanoparticles (NPs) (TiO_2, PbS, and ZnO) and rotaxanes, to functionalize the surfaces of low-dimensional nanomaterials, such as Si NWs, SWCNTs, and graphene.

Initially, we reported an SWCNTs/TiO_2 hybrid photoswitch (Figure 13b, left). TiO_2 quantum dots (QDs) have been extensively investigated in photoharvesting, photocatalysis, and some other studies.[186,187] UV irradiation generates free electrons (e^-)

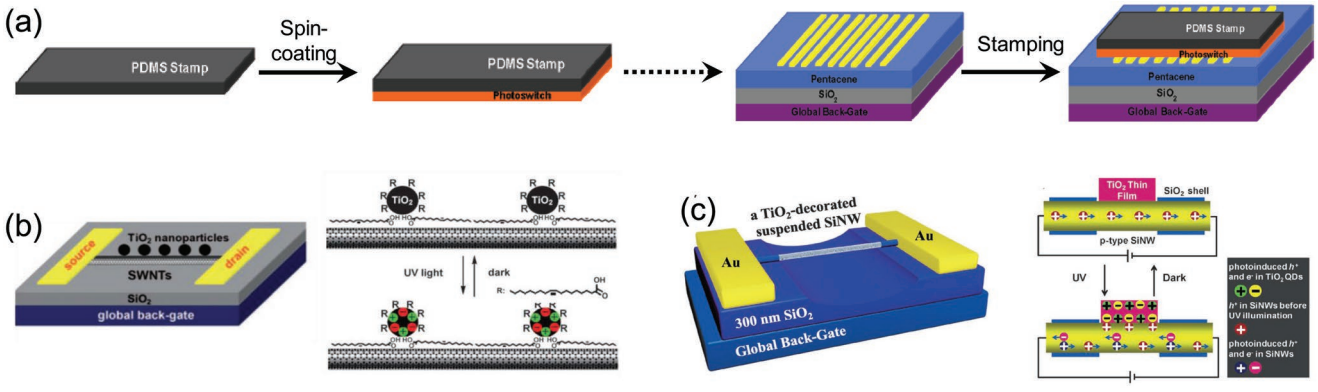

Figure 13. Modified ternary interfaces in 1D structures. a) Schematic illustration showing a noninvasive process to modify an active semiconductor layer with photochromic molecule layer. b) Representation of SWCNT transistors coated by TiO_2 NPs (left) and illustration of how these NPs affect the device characteristics with/without UV irradiation (right). c) Representation of individual TiO_2-decorated suspended Si NW transistors (left) and competitive photoswitching mechanisms of decorated Si NW transistors (right). (a) Reproduced with permission.[3] Copyright 2009, American Chemical Society. (b) Reproduced with permission.[2] Copyright 2009, Wiley-VCH. (c) Reproduced with permission.[6] Copyright 2013, Wiley-VCH.

and holes (h^+) in TiO_2, which could serve as the active sites on its surface (Figure 13b, right). UV-induced free electrons separate and migrate to the surface and produce scattering sites for hole carriers that flow through p-type tubes and lower the current. In contrast, the photoswitching effects of ambipolar CNTs are the mirror-image of those of p-type tubes.[188] Integrating SWCNTs and ZnO (bandgap: E_g = 3.37 eV) NPs, a tunable hybrid photodetector was fabricated with a responsivity of up to five orders of magnitude.[2] The ultrahigh light responsiveness of the device can be attributed to the inherent sensitivity of the nanosized SWCNT transistor and the synergistic effect of the SWCNT/ZnO interface. These results suggest that these SWCNT/NP hybrid materials are suitable for photodetection and photocatalysis applications.

Since silicon is the most widely used semiconductor material in today's electronic industry, combined with the semiconductor/NP hybridization strategy mentioned above, we used 1D Si NWs as a local probe, combined with TiO_2 QDs as the light antenna, to reveal the inherent charge transfer mechanism. (Figure 13c, left).[6] Typically, at the Si NWs/TiO_2 interface, UV radiation simultaneously activates the ground state electrons of Si NWs and TiO_2 QDs into an excited state. However, the former increases the carrier density in the conductive channel of Si NWs, whereas the latter has a different behavior depending on the type of Si NWs in the composites (Figure 13c, right). In p-type Si NWs, photoinduced free electrons of TiO_2 QDs generate active scattering sites for hole carriers of the Si NWs at the interface and reduce carrier mobility, thereby forming a competitive mechanism with significant bias dependence. In contrast, in n-type Si NWs, the photogenerated electrons of TiO_2 QDs work synergistically with the electron carriers of the Si NWs to produce a constant photocurrent. This sets the foundation for highly responsive reversible photosensing.

In addition to photosensing applications, it is of great importance to establish a practical platform for electrically detecting biomolecular interactions, with high sensitivity, stability, selectivity, and reversibility. FETs provide an attractive platform to realize this goal, owing to their ability to directly translate the interaction with target molecules taking place on the FET surface into readable electronic signals (detected directly), which allows for a more rapid and convenient sensing. Coupled to the 1D nature of Si NWs, Si NW-FETs have emerged as promising biosensors because of their high sensitivity and selectivity, real-time response, and label-free detection capabilities. Moreover, thanks to their excellent amorphous SiO_2 sheaths, Si NWs are especially appropriate for modification to build a ternary interface for specific chemical and biodetection (**Figure 14**a,b). Duan et al.[15] showed that Si NW-FETs can be used as affinity biosensors to monitor the binding affinities and kinetics of protein–ligand interactions (Figure 14c,d). Biotin was functionalized on the SiO_2 surface via an N-hydroxysuccinimide (NHS)-polyethylene glycol (PEG4)-biotin linker using succinimidyl ester chemistry of an amine-functionalized Si NWs. Thereafter, streptavidin was able to attach, and the electrical responses were recorded. Figure 14e presents the I_d–V_g characteristics for streptavidin binding with biotin on the Si NW-FET, resulting in a parallel *I*–*V* curve shifting to a lower voltage because of the protein's negative charge. The kinetics were investigated in a series of time-lapse measurements for streptavidin solutions ranging in concentration from 200×10^{-15} to 2×10^{-9} M (Figure 14f,g).

In particular, the detection of biological system interactions at the molecular level is critical for basic biology, medical chemistry, clinical diagnosis, and drug discovery. To this end, several methods based on nanomaterials and novel structures have been successfully developed for the manufacture of single-molecule biosensors, including molecular junctions,[190] Si NWs,[191] CNTs,[192] and nanopores.[193] In the past few years, our group has developed a point decoration strategy for Si NWs, by integrating top-down lithography with bottom-up chemical reactions (**Figure 15**a). To enable the molecular scale point decoration, high-resolution electron beam lithography is needed to open a narrow window perpendicular to the Si NWs on the surface, followed by wet etching by HF/NH_4F buffer solution through the window, to expose the crystalline silicon core. This process yields a hydrogen-terminated silicon trench at a nanoscale size, which is orthogonal to the hydroxyl-terminated sheath and is suitable for photochemical hydrosilylation chemistry. Thereafter, biomolecules such as proteins and DNA can be functionalized on the nanogap, at the molecular level.

The reliable Si NW-FET biosensor platform is suitable for real-time label-free detection of influenza viruses, with high selectivity and single-molecule sensitivity (Figure 15b–d). It is also capable of real-time detection of single molecule dynamic events, such as DNA hybridization (Figure 15e,f),[7,9] adenosine triphosphatase hydrolysis,[8] and antigen–antibody interactions.[189] These advantages imply that it is a promising platform for exploring the dynamics of stochastic processes in biological systems, to improve accurate molecular and even point-of-care clinical diagnosis (Figure 15f). Furthermore, by integrating the Si NW-FET sensor with microfluidics and bioaerosol–hydrosol air sampling technology, a practical airborne virus (H1N1, H3N2) sensing platform can be built.[4] The specific interaction between the antibody and antigen (influenza viruses) changes the carrier density at the interface. This allows the detection of discrete NW conductance changes in seconds.

4.2. Ternary Interfaces in Graphene Hybrid Structures

Since its introduction, SLG and its hybrids have been widely used in the fabrication of sensing elements because of their superior properties, such as single-atom thick 2D conjugated structures, high electrical conductivity, and large specific surface area.[194] A significant advantage of SLG as a sensing element is its 2D nature, which exposes every carbon atom on the surface to the environment; hence, any stimuli in the environment can cause dramatic electrical responses.[195] However, some inherent drawbacks hamper the method of applying graphene transistors as a platform for chemical or photodetection applications. First, it lacks selectivity because the analytes are always physically absorbed on the graphene surface, causing doping or gate effects that lead to current changes. Second, the responsivity of graphene-based photodetectors is limited by the limited light absorption and the absence of a gain mechanism that can generate multiple charge carriers from one incident photon. One solution to these is to choose defective graphene species such as graphene oxides, or graphene nanoribbons as testing beds, at the cost of electrical properties.

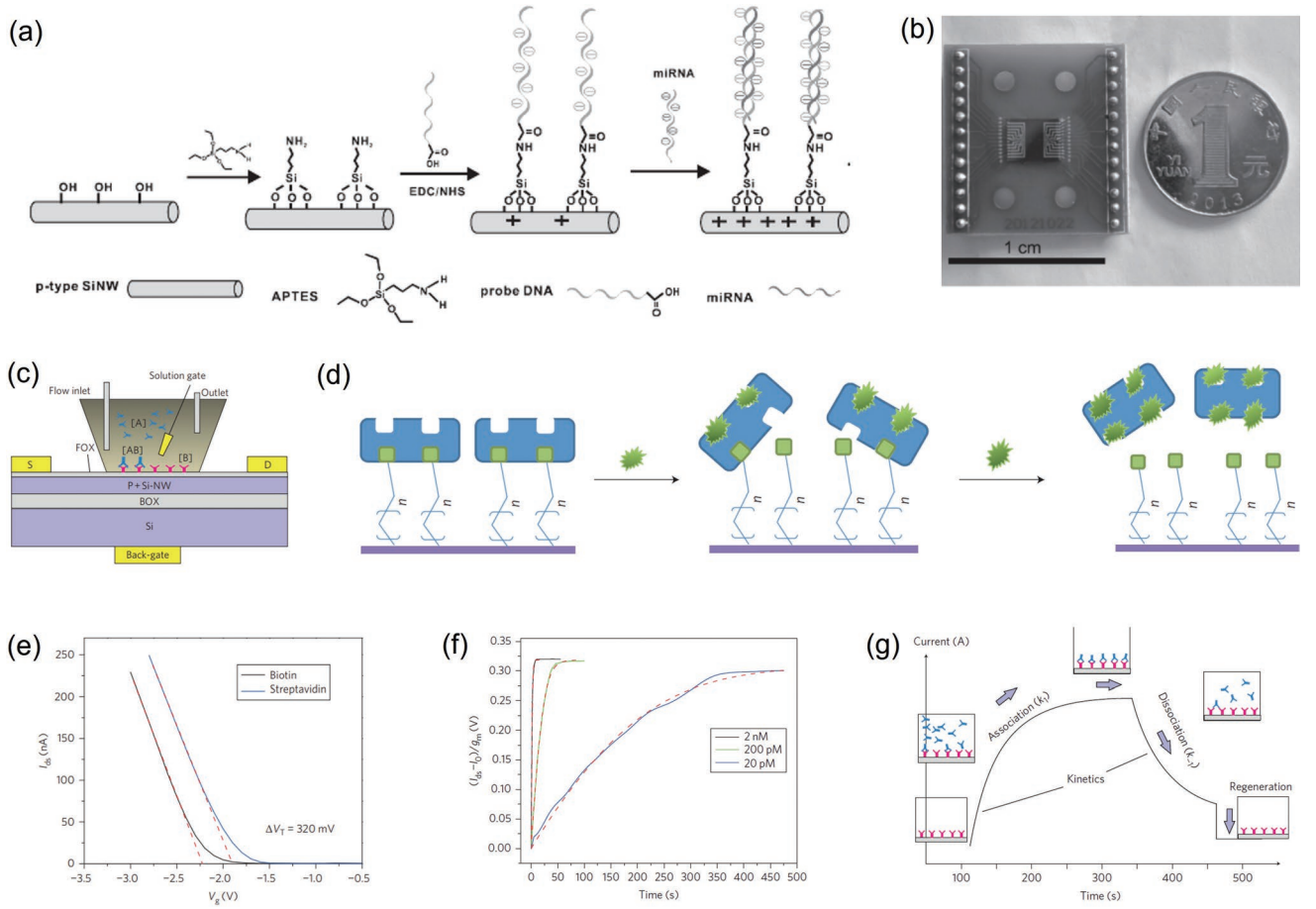

Figure 14. Si NW-FET based sensors. a) Schematic illustration showing the fabrication process of a Si NW-FET sensor and electrical direct detection mechanism of miRNA molecules. b) Photograph of a complete Si NW-FET chip. c) Schematic of the Si NW-FET biosensor setup. d) Schematic of the competitive dissociation processes of streptavidin from the biotin-functionalized surface. e) I_d–V_g characteristics of HMGB1-DNA binding measured by Si NW-FETs. f) Real-time sensor responses of biotin-streptavidin binding. g) Typical schematic binding cycle for measurements obtained by using the Si NW-FET biosensor. (a,b) Reproduced with permission.[16] Copyright 2014, Wiley-VCH. (c–g) Reproduced with permission.[15] Copyright 2012, Nature Publishing Group.

To solve the first problem, we[11,13,14] and some other groups[17,18] modified the graphene/environment interface with stimuli-active components to fabricate graphene-based hybrid chemical sensors or photodetectors with highly sensitive responses to external stimuli. A variety of graphene composites,[196] such as graphene/polymer composites, have also been used as active sensing materials to improve the performances of graphene-based gas sensors.[197,198] Noble metal NPs such as palladium and platinum NPs were deposited onto graphene layers to catalyze the gas reactions and improve the sensing performance. In particular, for graphene/metal oxide composites, the adsorption of oxygen on the surface of the metal oxides is crucial to achieve a higher sensing response. A facile fabrication of graphene/TiO_2 hybrid oxygen gas (O_2) sensors has been realized in our lab (**Figure 16**a).[10,12] Controlling the photoactivity of TiO_2 allows fast and significant photoswitching effects in graphene/TiO_2 hybrid devices, to realize a reversible and linear electrical sensitivity toward O_2. The unique sensitivity of these devices is attributed to the synergetic effect at the ternary interface composed of TiO_2 as a photoactive semiconductor, O_2 as an electron acceptor, and graphene as an electron transporter.

For the second problem, to improve the limited optical absorption level of SLG, hybrid devices or heterojunction phototransistors were constructed in which graphene is composited with another photosensitive material. This approach was adopted using semiconducting QDs as sensitizers in graphene FETs (Figure 16b).[17] QD optical absorption leads to photoexcited free charge carriers, with the holes as active centers, over the entire nanocrystal. Our group immobilized PbS QDs, which are light absorbers, on graphene surfaces.[199] Under irradiation, PbS QDs generate free carriers, electrons and holes, as the active centers, over the entire surface of the nanocrystals. Using graphene as a local probe, we found that photoinduced holes can be rapidly transferred from PbS to graphene. It is worth noting that when different gate fields are applied, the symmetric mirror-imaging photoswitching effect is rationally realized using a single pristine ambipolar SLG.

In addition to NPs, some other easy and efficient ways to covalently modify the graphene surface, such as electrochemistry and gas-phase reactions, have been investigated.[200,201] Covalent modification might induce bandgap opening in graphene and modulate its transport properties in a simple and

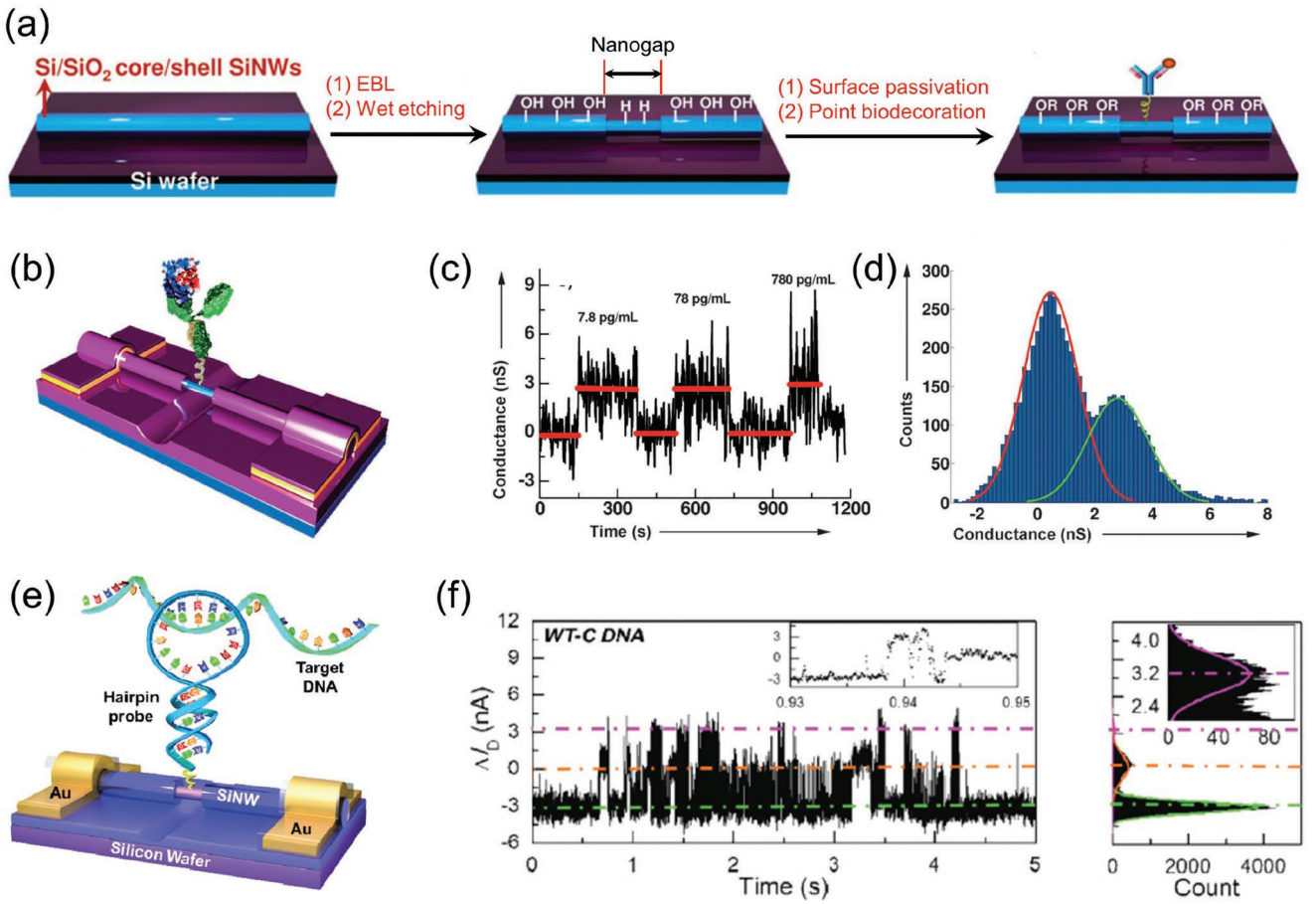

Figure 15. a) Schematic illustration showing a three-step process to fabricate Si NW-FET based single-molecule biosensors. b) Representation of single-molecule virus biosensor formed by point decoration of Si NWs. c) Net conductance changes versus time of the single-molecule device upon increased antigen concentrations. d) Conductance-based histograms fit to Gaussian distributions. e) Representation of Si NWs single-molecule biosensor to detect the hybridization process between the hairpin probe and the target DNA. f) Current fluctuations of a representative single hairpin DNA-decorated Si NWs biosensor measured in a phosphate-buffered saline (PBS) solution containing 1×10^{-6} M wild-type complementary target DNA (WT-C DNA). Insets show representative data over a short time interval. Right panel shows the corresponding histograms of current values, revealing three Gaussian peaks in conductance. (a–d) Reproduced with permission.[189] Copyright 2014, Wiley-VCH. (e,f) Reproduced with permission.[9] Copyright 2017, Wiley-VCH.

controllable way, but at the cost of its electrical properties. In a different way, we demonstrated a noncovalent modification of graphene with 1-pyrenebutanoic acid-anchored redox-bistable[2]rotaxane, which binds with the graphene surface by means of π–π stacking interactions (Figure 16c).[11] This multifunctional optoelectronic device displayed symmetric mirror-image photoswitching with a nonvolatile memory effect. The phenomenon can be attributed to the rational control of the synergistic effects of electrostatic gating and chemical n-doping at the interface, which is caused by the light-induced translational motions of the bistable [2]rotaxane rings. These multilevel changes in the device properties and electrical signals enable it to be integrated into current circuit technologies to achieve basic logic computing functions.

As mentioned above, graphene/acceptor/environment ternary interfaces are sensitive and efficient enough for photocarrier generation, separation, and transport. We tried to engineer the interface to make an energy-harvesting device. A photodiode is one of the most fundamental structures for photovoltaic solar cells. It is composed of metal/semiconductor heterostructures or homo/heterostructures between different semiconductors. Typically, in photodiode-based devices, two pairs of hole/electron selective conductor layers and collecting electrodes are constructed on each side of the semiconductor layers. Upon light illumination, electron–hole pairs are created in the semiconductor layer, after which, they are separated at the heterojunction interfaces and transported in opposite directions.[202] To promote the development of this field and enable the development of high-efficiency low-cost photovoltaic and optoelectronic device architectures, ingenious and reliable interface designs for highly efficient separation and transmission of photogenerated carriers are required.[203,204] In this regard, our group has developed a unique heterostructure photovoltaic diode with an all-solid-state ternary interface (TiO_2/SLG/dye), which is composed of a TiO_2 electron-collecting layer, SLG hole-transporting layer, and monolayer of dye molecules (**Figure 17**a).[13] Different from the conventional photovoltaic conversion process, in our photovoltaic device, both the electrons and holes generated by photoexcitation can tunnel into the graphene along the same direction, but only the electrons

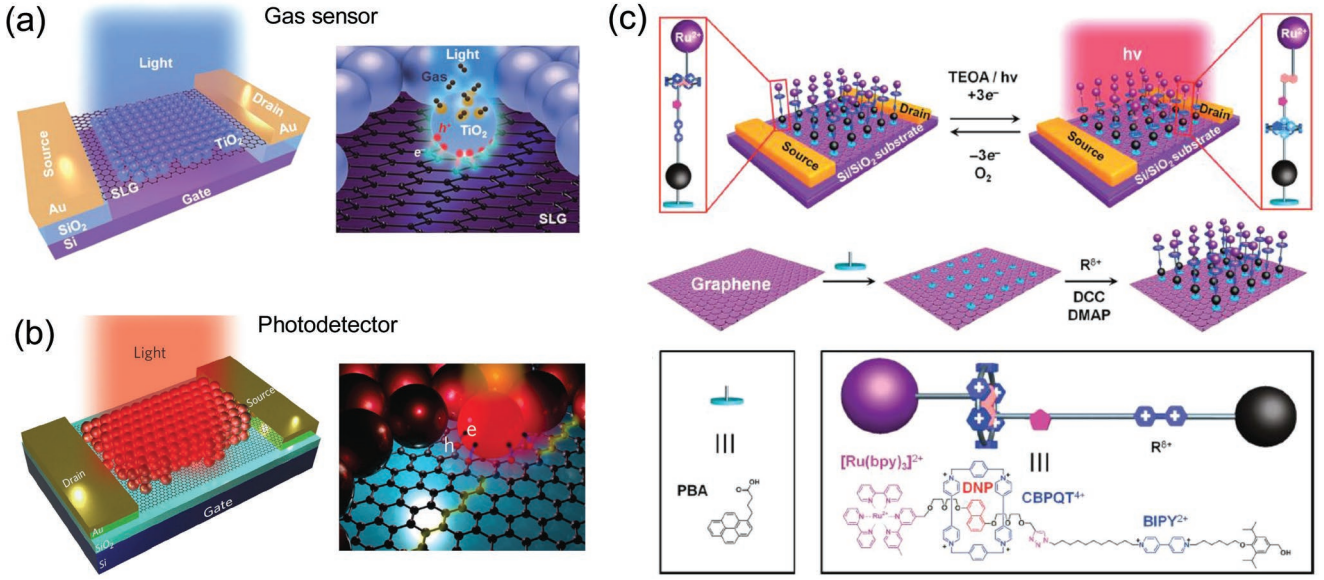

Figure 16. Ternary interfaces in graphene hybrid structure. a) Schematic illustration of a multifunctional graphene/TiO_2 hybrid transistor, where TiO_2 QDs were immobilized onto a suspended graphene flake (left) and the exposure of TiO_2 QDs to light and gases can affect the graphene's conductance (right). h, hole; e, electron. b) Schematic illustration showing a graphene/PbS QDs hybrid phototransistor (left) and that the QDs absorb light, transfer the photoexcited holes to graphene, and finally dope the graphene and produce the photoresponse (right). c) Schematic illustration showing a graphene transistor decorate with light switchable [2]rotaxane. (a) Reproduced with permission.[12] Copyright 2016, Wiley-VCH. (b) Reproduced with permission.[17] Copyright 2012, Nature Publishing Group. (c) Reproduced with permission.[11] Copyright 2013, Wiley-VCH.

show a highly efficient ballistic transport to the TiO_2 transport layer (Figure 17b). The efficiency of photogenerated charge separation at the interface is determined by the competition between efficient charge transfer and inefficient loss processes. This ipsilateral selective electron tunneling (ISET) mechanism results in an ultrahigh absorbed photon-to-current efficiency (Figure 17c,d).

From another point of view, in this structure, the Schottky junction formed between graphene and TiO_2 enables the separation of photogenerated carriers without an external power

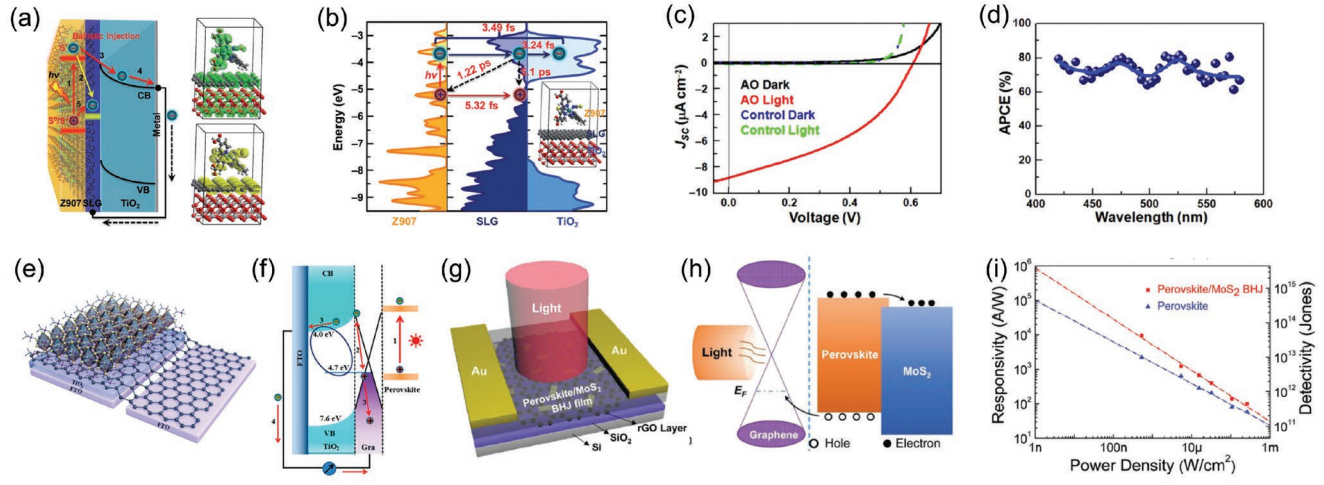

Figure 17. All-solid-state ternary interface in a photovoltaic diode device. a) Schematic illustration showing the photovoltaic effect at an all-solid-state ternary interface of a photovoltaic diode. b) The calculated projected density-of-states (PDOS) spectra for Z907, SLG, and TiO_2, showing the electronic structures of the heterointerface. c) *I–V* characteristics of the device measured in the dark (black solid line) and under visible (>420 nm) illumination (red solid line). For comparison, a control device without the dye was also studied in the dark (blue dashed line) and under the same illumination conditions (bright green dashed line). d) The absorbed photon-to-current conversion efficiency (APCE) spectrum showing an ultrahigh internal quantum efficiency of ≈80%. e) Schematic illustration showing the structure of a perovskite/graphene/TiO_2/FTO photodetector. f) Schematic illustration showing the mechanism of dynamic processes at the ternary interface in the photodetector. g) Schematic illustration showing hybrid photodetector. h) Energy level diagram of the perovskite/MoS_2/rGO hybrid structure. i) Dependences of photoresponsivity and detectivity on the incident light power density for the photodetector. (a–d) Reproduced with permission.[14] Copyright 2017, Wiley-VCH. (e,f) Reproduced with permission.[18] Copyright 2017, American Chemical Society. (g–i) Reproduced with permission.[19] Copyright 2018, Wiley-VCH.

source. Therefore, such a device structure can be used for detecting light irradiation, for example, a Schottky junction formed between graphene and photosensitive perovskite. It is possible to efficiently separate and transport photogenerated excitons at the graphene/perovskite heterointerface. This sets the foundation for self-powered photodetectors with a high sensitivity and response speed (Figure 17e).[18] Figure 17f shows the transporting mechanism of the photodetector. Upon light illumination, excitons with low binding energy are generated in the perovskite layer, which then dissociate into free electrons and holes. Thereafter, both electrons and holes can be transferred from the perovskite to graphene, at this ternary interface. The electrons on the graphene are transferred directly to TiO_2, because of the Schottky field between graphene and TiO_2, and are finally collected by the fluorine doped tin oxide (FTO) electrode. However, the holes, which remain in the graphene, are transferred and collected by another FTO electrode, in the end. Thus, graphene plays a crucial role in the self-powered photodetector. Based on the ISET charge separation mechanism at the ternary interface, this photovoltaic device has a high photo-to-current conversion efficiency and is expected to be applied as a fundamental device architecture for photovoltaic solar cells, photodetectors, and other novel optoelectronic devices. Peng et al.[19] reported a similar strategy, utilizing a perovskite/MoS_2 heterojunction as the photosensitizer and a rGO layer as the conducting channel, to realize high-performance photodetectors (Figure 17g). The perovskite/MoS_2 heterojunction can significantly suppress the recombination of photoinduced carriers because of the selective electron trapping in the MoS_2 layer. As a result, the photoinduced hole transfer from perovskite to rGO is facilitated, greatly increasing the photocurrent (Figure 17h). The hybrid photodetectors show a high responsivity of 1.08×10^4 A W^{-1} and a high detectivity of 4.28×10^{13} Jones (Figure 17i).

5. Concluding Remarks and Outlook

Heterogeneous interfaces including semiconductor/electrode interfaces, semiconductor/dielectric interfaces, interfaces within semiconductor hybrids, and ternary interfaces in sensors are thoroughly summarized in this review with a particular focus on improving the device performance, realizing new functions, and reducing fabrication cost. Despite these achievements, both opportunities and challenges for controlling interfacial charge transport still remain:

1) *Interface Modification Method*: Several methods have been developed to modify and functionalize electrodes as well as dielectric surface; however, it is hard to say that these methods are perfect. New chemistry should be developed to enrich the pool of materials, which includes new anchors and modification methods, as well as new semiconductors with high stability, biodegradability, and functionality.
2) *Binary Interfaces*: The four most important components, namely the semiconductor, dielectric, electrodes, and environment, as well as the binary interfaces within them, have attracted the most attention in the past several years. As mentioned in Section 3, although these interfaces can be easily modified, their integration with 2D materials still remains a big challenge. 2D materials could serve as excellent epitaxial substrates for the growth of high-crystallinity OSC films, forming well-ordered junctions, with improved transport performance. The following two points at OSCs/2D material interfaces that cannot be found in all-2D heterostructures can be further envisioned: i) Singlet fission of OSCs might improve the optoelectronic performance beyond the Shockley–Queisser limit, by the use of 2D materials to extract the multiple carriers generated by the singlet fission at the interface. ii) Excited electrons in OSCs would maintain the spin state for a long period of time and combine with the spin and pseudospin properties of TMD crystals to produce next-generation spintronic devices. Considering all this, more efforts should be devoted to explore mixed-dimensional semiconductors and improve the understanding of interfacial carrier dynamics, in order to enhance the performance and multifunctionality.
3) *Ternary Interfaces and Beyond*: Among strategies for the functionalization of optoelectronic devices, the approach through interface engineering involving ternary and more interfaces seemingly exhibited intrinsic advantages over binary interface control. Multifunctionality can even be installed into the device with holistic design. The synergistic effect can make such device a promising platform for future application and commercialization. However, the lack of efficient functionalization methods and low integration degree affects the massive expansion of this field. Recently, the integration of biointerfaces with flexible bioelectronics opens up a brand new direction which includes flexible, biocompatible, and biodegradable materials design as well as device engineering to provide more reliable device operation. Some new concept such as optogenetics has also been transplanted to design more complicated functional interfaces and sensors. However, there is still a long way to go before they can really be used for real applications.

Acknowledgements

W.Z. and H.C. contributed equally to this work. The authors acknowledge primary financial supports from National Key R&D Program of China (2017YFA0204901), the National Natural Science Foundation of China (21727806), the Natural Science Foundation of Beijing (Z181100004418003), and the interdisciplinary medicine Seed Fund of Peking University.

Conflict of Interest

The authors declare no conflict of interest.

Keywords

charge transport, functional devices, interface engineering, optoelectronic devices

Received: August 16, 2018
Revised: October 26, 2018
Published online:

[1] C. Liu, Y. Xu, Y. Y. Noh, *Mater. Today* **2015**, *18*, 79.
[2] S. Liu, J. Ye, Y. Cao, Q. Shen, Z. Liu, L. Qi, X. Guo, *Small* **2009**, *5*, 2371.
[3] Q. Shen, Y. Cao, S. Liu, M. L. Steigerwald, X. Guo, *J. Phys. Chem. C* **2009**, *113*, 10807.
[4] L. Chen, A. Feng, M. Wang, J. Liu, W. Hong, X. Guo, D. Xiang, *Sci. China: Chem.* **2018**, *61*, 1368.
[5] F. Shen, J. Wang, Z. Xu, Y. Wu, Q. Chen, X. Li, X. Jie, L. Li, M. Yao, X. Guo, T. Zhu, *Nano Lett.* **2012**, *12*, 3722.
[6] J. Wang, Z. Wang, Q. Li, L. Gan, X. Xu, L. Li, X. Guo, *Angew. Chem., Int. Ed.* **2013**, *52*, 3369.
[7] G. He, J. Li, H. Ci, C. Qi, X. Guo, *Angew. Chem., Int. Ed.* **2016**, *55*, 9036.
[8] J. Li, G. He, U. Hiroshi, W. Liu, H. Noji, C. Qi, X. Guo, *ACS Nano* **2017**, *11*, 12789.
[9] G. He, J. Li, C. Qi, X. Guo, *Adv. Sci.* **2017**, *4*, 1700158.
[10] Q. Wang, X. F. Guo, L. C. Cai, Y. Cao, L. Gan, S. Liu, Z. X. Wang, H. T. Zhang, L. D. Li, *Chem. Sci.* **2011**, *2*, 1860.
[11] C. Jia, H. Li, J. Jiang, J. Wang, H. Chen, D. Cao, J. F. Stoddart, X. Guo, *Adv. Mater.* **2013**, *25*, 6752.
[12] C. C. Jia, Q. Wang, N. Xin, J. Zhou, Y. Gong, L. D. Li, Q. Sun, X. F. Guo, *Adv. Mater. Technol.* **2016**, *1*, 1600067.
[13] C. Jia, W. Ma, C. Gu, H. Chen, H. Yu, X. Li, F. Zhang, L. Gu, A. Xia, X. Hou, S. Meng, X. Guo, *Nano Lett.* **2016**, *16*, 3600.
[14] C. Jia, W. Ma, J. Guan, C. Gu, X. Li, L. Meng, Y. Gong, S. Meng, X. Guo, *Adv. Electron. Mater.* **2017**, *3*, 1700211.
[15] X. Duan, Y. Li, N. K. Rajan, D. A. Routenberg, Y. Modis, M. A. Reed, *Nat. Nanotechnol.* **2012**, *7*, 401.
[16] N. Lu, A. Gao, P. Dai, S. Song, C. Fan, Y. Wang, T. Li, *Small* **2014**, *10*, 2022.
[17] G. Konstantatos, M. Badioli, L. Gaudreau, J. Osmond, M. Bernechea, F. P. Garcia de Arquer, F. Gatti, F. H. Koppens, *Nat. Nanotechnol.* **2012**, *7*, 363.
[18] J. Li, S. Yuan, G. Tang, G. Li, D. Liu, J. Li, X. Hu, Y. Liu, J. Li, Z. Yang, S. F. Liu, Z. Liu, F. Gao, F. Yan, *ACS Appl. Mater. Interfaces* **2017**, *9*, 42779.
[19] Z.-Y. Peng, J.-L. Xu, J.-Y. Zhang, X. Gao, S.-D. Wang, *Adv. Mater. Interfaces* **2018**, *5*, 1800505.
[20] Y. Don Park, J. A. Lim, H. S. Lee, K. Cho, *Mater. Today* **2007**, *10*, 46.
[21] C. A. Di, Y. Liu, G. Yu, D. Zhu, *Acc. Chem. Res.* **2009**, *42*, 1573.
[22] H. Ma, H. L. Yip, F. Huang, A. K. Y. Jen, *Adv. Funct. Mater.* **2010**, *20*, 1371.
[23] H. Dong, L. Jiang, W. Hu, *Phys. Chem. Chem. Phys.* **2012**, *14*, 14165.
[24] B. Lussem, C. M. Keum, D. Kasemann, B. Naab, Z. Bao, K. Leo, *Chem. Rev.* **2016**, *116*, 13714.
[25] S. Casalini, C. A. Bortolotti, F. Leonardi, F. Biscarini, *Chem. Soc. Rev.* **2017**, *46*, 40.
[26] D. Q. Liu, Q. Miao, *Mater. Chem. Front.* **2018**, *2*, 11.
[27] N. Seiki, Y. Shoji, T. Kajitani, F. Ishiwari, A. Kosaka, T. Hikima, M. Takata, T. Someya, T. Fukushima, *Science* **2015**, *348*, 1122.
[28] T. Yokota, T. Kajitani, R. Shidachi, T. Tokuhara, M. Kaltenbrunner, Y. Shoji, F. Ishiwari, T. Sekitani, T. Fukushima, T. Someya, *Nat. Nanotechnol.* **2018**, *13*, 139.
[29] C. W. Chu, S. H. Li, C. W. Chen, V. Shrotriya, Y. Yang, *Appl. Phys. Lett.* **2005**, *87*, 193508.
[30] Y. Yi, P. E. Jeon, H. Lee, K. Han, H. S. Kim, K. Jeong, S. W. Cho, *J. Chem. Phys.* **2009**, *130*, 094704.
[31] S. Cho, J. H. Seo, K. Lee, A. J. Heeger, *Adv. Funct. Mater.* **2009**, *19*, 1459.
[32] Y. H. Gao, Y. D. Shao, L. J. Yan, H. Li, Y. T. Su, H. Meng, X. W. Wang, *Adv. Funct. Mater.* **2016**, *26*, 4456.
[33] T. Minari, P. Darmawan, C. Liu, Y. Li, Y. Xu, K. Tsukagoshi, *Appl. Phys. Lett.* **2012**, *100*, 093303.
[34] N. K. Kim, D. Khim, Y. Xu, S. H. Lee, M. Kang, J. Kim, A. Facchetti, Y. Y. Noh, D. Y. Kim, *ACS Appl. Mater. Interfaces* **2014**, *6*, 9614.
[35] K. J. Baeg, J. Kim, D. Khim, M. Caironi, D. Y. Kim, I. K. You, J. R. Quinn, A. Facchetti, Y. Y. Noh, *ACS Appl. Mater. Interfaces* **2011**, *3*, 3205.
[36] Y. Xu, H. Sun, E. Y. Shin, Y. F. Lin, W. Li, Y. Y. Noh, *Adv. Mater.* **2016**, *28*, 8531.
[37] U. Zschieschang, M. J. Kang, K. Takimiya, T. Sekitani, T. Someya, T. W. Canzler, A. Werner, J. Blochwitz-Nimoth, H. Klauk, *J. Mater. Chem.* **2012**, *22*, 4273.
[38] J. L. Hou, D. Kasemann, J. Widmer, A. A. Gunther, B. Lussem, K. Leo, *Appl. Phys. Lett.* **2016**, *108*, 103303.
[39] Y. Zhou, C. Fuentes-Hernandez, J. Shim, J. Meyer, A. J. Giordano, H. Li, P. Winget, T. Papadopoulos, H. Cheun, J. Kim, M. Fenoll, A. Dindar, W. Haske, E. Najafabadi, T. M. Khan, H. Sojoudi, S. Barlow, S. Graham, J. L. Bredas, S. R. Marder, A. Kahn, B. Kippelen, *Science* **2012**, *336*, 327.
[40] J. Meyer, K. Zilberberg, T. Riedl, A. Kahn, *J. Appl. Phys.* **2011**, *110*, 033710.
[41] M. T. Greiner, L. Chai, M. G. Helander, W. M. Tang, Z. H. Lu, *Adv. Funct. Mater.* **2012**, *22*, 4557.
[42] R. Winter, M. S. Hammer, C. Deibel, J. Pflaum, *Appl. Phys. Lett.* **2009**, *95*, 263313.
[43] M. L. Tietze, P. Pahner, K. Schmidt, K. Leo, B. Lussem, *Adv. Funct. Mater.* **2015**, *25*, 2701.
[44] A. A. Gunther, M. Sawatzki, P. Formanek, D. Kasemann, K. Leo, *Adv. Funct. Mater.* **2016**, *26*, 768.
[45] C. R. Arroyo, E. Leary, A. Castellanos-Gomez, G. Rubio-Bollinger, M. T. Gonzalez, N. Agrait, *J. Am. Chem. Soc.* **2011**, *133*, 14313.
[46] H. Li, T. A. Su, V. Zhang, M. L. Steigerwald, C. Nuckolls, L. Venkataraman, *J. Am. Chem. Soc.* **2015**, *137*, 5028.
[47] T. A. Su, M. Neupane, M. L. Steigerwald, L. Venkataraman, C. Nuckolls, *Nat. Rev. Mater.* **2016**, *1*, 16002.
[48] H. Hakkinen, *Nat. Chem.* **2012**, *4*, 443.
[49] P. Maksymovych, O. Voznyy, D. B. Dougherty, D. C. Sorescu, J. T. Yates, *Prog. Surf. Sci.* **2010**, *85*, 206.
[50] H. Grönbeck, A. Curioni, W. Andreoni, *J. Am. Chem. Soc.* **2000**, *122*, 3839.
[51] M. T. Gonzalez, E. Leary, R. Garcia, P. Verma, M. A. Herranz, G. Rubio-Bollinger, N. Martin, N. Agrait, *J. Phys. Chem. C* **2011**, *115*, 17973.
[52] A. Operamolla, A. Punzi, G. M. Farinola, *Asian J. Org. Chem.* **2017**, *6*, 120.
[53] J. M. Tour, L. Jones, D. L. Pearson, J. J. S. Lamba, T. P. Burgin, G. M. Whitesides, D. L. Allara, A. N. Parikh, S. Atre, *J. Am. Chem. Soc.* **1995**, *117*, 9529.
[54] E. Kaletova, A. Kohutova, J. Hajduch, J. Kaleta, Z. Bastl, L. Pospisil, I. Stibor, T. F. Magnera, J. Michl, *J. Am. Chem. Soc.* **2015**, *137*, 12086.
[55] D. Khobragade, E. S. Stensrud, M. Mucha, J. R. Smith, R. Pohl, I. Stibor, J. Michl, *Langmuir* **2010**, *26*, 8483.
[56] W. Hong, H. Li, S. X. Liu, Y. Fu, J. Li, V. Kaliginedi, S. Decurtins, T. Wandlowski, *J. Am. Chem. Soc.* **2012**, *134*, 19425.
[57] C. Saby, B. Ortiz, G. Y. Champagne, D. Bélanger, *Langmuir* **1997**, *13*, 6805.
[58] A. Lv, M. Freitag, K. M. Chepiga, A. H. Schafer, F. Glorius, L. Chi, *Angew. Chem., Int. Ed.* **2018**, *57*, 4792.
[59] N. Moller, A. Ruhling, S. Lamping, T. Hellwig, C. Fallnich, B. J. Ravoo, F. Glorius, *Angew. Chem., Int. Ed.* **2017**, *56*, 4356.
[60] G. Wang, A. Ruhling, S. Amirjalayer, M. Knor, J. B. Ernst, C. Richter, H. J. Gao, A. Timmer, H. Y. Gao, N. L. Doltsinis, F. Glorius, H. Fuchs, *Nat. Chem.* **2017**, *9*, 152.
[61] S. Engel, E. C. Fritz, B. J. Ravoo, *Chem. Soc. Rev.* **2017**, *46*, 2057.
[62] H. Chen, X. Guo, *Small* **2013**, *9*, 1144.
[63] S. A. DiBenedetto, A. Facchetti, M. A. Ratner, T. J. Marks, *Adv. Mater.* **2009**, *21*, 1407.
[64] M. E. McGovern, K. M. R. Kallury, M. Thompson, *Langmuir* **1994**, *10*, 3607.

[65] S. Kobayashi, T. Nishikawa, T. Takenobu, S. Mori, T. Shimoda, T. Mitani, H. Shimotani, N. Yoshimoto, S. Ogawa, Y. Iwasa, *Nat. Mater.* **2004**, *3*, 317.
[66] D. Boudinet, M. Benwadih, S. Altazin, J.-M. Verilhac, E. De Vito, C. Serbutoviez, G. Horowitz, A. Facchetti, *J. Am. Chem. Soc.* **2011**, *133*, 9968.
[67] B. Wang, G. Di Carlo, R. Turrisi, L. Zeng, K. Stallings, W. Huang, M. J. Bedzyk, L. Beverina, T. J. Marks, A. Facchetti, *Chem. Mater.* **2017**, *29*, 9974.
[68] F. Schreiber, *Prog. Surf. Sci.* **2000**, *65*, 151.
[69] A. Ulman, *Chem. Rev.* **1996**, *96*, 1533.
[70] D. L. Angst, G. W. Simmons, *Langmuir* **1991**, *7*, 2236.
[71] A. Y. Fadeev, T. J. McCarthy, *Langmuir* **2000**, *16*, 7268.
[72] S. Onclin, B. J. Ravoo, D. N. Reinhoudt, *Angew. Chem., Int. Ed.* **2005**, *44*, 6282.
[73] N. Benson, A. Gassmann, E. Mankel, T. Mayer, C. Melzer, R. Schmechel, H. von Seggern, *J. Appl. Phys.* **2008**, *104*, 054505.
[74] N. Benson, C. Melzer, R. Schmechel, H. von Seggern, *Phys. Status Solidi A* **2008**, *205*, 475.
[75] L. L. Chua, P. K. H. Ho, H. Sirringhaus, R. H. Friend, *Appl. Phys. Lett.* **2004**, *84*, 3400.
[76] L.-L. Chua, J. Zaumseil, J.-F. Chang, E. C. W. Ou, P. K. H. Ho, H. Sirringhaus, R. H. Friend, *Nature* **2005**, *434*, 194.
[77] L. Bu, M. Hu, W. Lu, Z. Wang, G. Lu, *Adv. Mater.* **2018**, *30*, 1704695.
[78] C. Kim, A. Facchetti, T. J. Marks, *Science* **2007**, *318*, 76.
[79] C. Kim, J. R. Quinn, A. Facchetti, T. J. Marks, *Adv. Mater.* **2010**, *22*, 342.
[80] C. D. Dimitrakopoulos, I. Kymissis, S. Purushothaman, D. A. Neumayer, P. R. Duncombe, R. B. Laibowitz, *Adv. Mater.* **1999**, *11*, 1372.
[81] H. Chen, N. Cheng, W. Ma, M. Li, S. Hu, L. Gu, S. Meng, X. Guo, *ACS Nano* **2016**, *10*, 436.
[82] Y. Mei, P. J. Diemer, M. R. Niazi, R. K. Hallani, K. Jarolimek, C. S. Day, C. Risko, J. E. Anthony, A. Amassian, O. D. Jurchescu, *Proc. Natl. Acad. Sci. USA* **2017**, *114*, E6739.
[83] J. H. Li, D. Q. Liu, Q. Miao, F. Yan, *J. Mater. Chem.* **2012**, *22*, 15998.
[84] S. H. Kim, S. Y. Yang, K. Shin, H. Jeon, J. W. Lee, K. P. Hong, C. E. Park, *Appl. Phys. Lett.* **2006**, *89*, 183516.
[85] M. Guo, T. Hayakawa, M. A. Kakimoto, T. Goodson, 3rd, *J. Phys. Chem. B* **2011**, *115*, 13419.
[86] G. He, L. Q. Zhu, Z. Q. Sun, Q. Wan, L. D. Zhang, *Prog. Mater. Sci.* **2011**, *56*, 475.
[87] Y. G. Ha, K. Everaerts, M. C. Hersam, T. J. Marks, *Acc. Chem. Res.* **2014**, *47*, 1019.
[88] B. Wang, W. Huang, L. Chi, M. Al-Hashimi, T. J. Marks, A. Facchetti, *Chem. Rev.* **2018**, *118*, 5690.
[89] B. Lussem, M. L. Tietze, H. Kleemann, C. Hossbach, J. W. Bartha, A. Zakhidov, K. Leo, *Nat. Commun.* **2013**, *4*, 2775.
[90] X. Zhang, Z. Shao, X. Zhang, Y. He, J. Jie, *Adv. Mater.* **2016**, *28*, 10409.
[91] F. Zhang, X. Dai, W. Zhu, H. Chung, Y. Diao, *Adv. Mater.* **2017**, *29*, 1700411.
[92] I. E. Jacobs, A. J. Moule, *Adv. Mater.* **2017**, *29*, 1703063.
[93] B. H. Lee, G. C. Bazan, A. J. Heeger, *Adv. Mater.* **2016**, *28*, 57.
[94] P. Pingel, R. Schwarzl, D. Neher, *Appl. Phys. Lett.* **2012**, *100*, 143303.
[95] G. Lu, J. Blakesley, S. Himmelberger, P. Pingel, J. Frisch, I. Lieberwirth, I. Salzmann, M. Oehzelt, R. Di Pietro, A. Salleo, N. Koch, D. Neher, *Nat. Commun.* **2013**, *4*, 1588.
[96] C. Liu, J. Jang, Y. Xu, H. J. Kim, D. Khim, W. T. Park, Y. Y. Noh, J. J. Kim, *Adv. Funct. Mater.* **2015**, *25*, 758.
[97] L. Hu, T. F. Liu, J. S. Duan, X. Y. Ma, C. W. Ge, Y. Y. Jiang, F. Qin, S. X. Xiong, F. Y. Jiang, B. Hu, X. K. Gao, Y. P. Yi, Y. H. Zhou, *Adv. Funct. Mater.* **2017**, *27*, 1703254.
[98] J. Panidi, A. F. Paterson, D. Khim, Z. Fei, Y. Han, L. Tsetseris, G. Vourlias, P. A. Patsalas, M. Heeney, T. D. Anthopoulos, *Adv. Sci.* **2018**, *5*, 1700290.
[99] Y. Hu, Z. D. Rengert, C. McDowell, M. J. Ford, M. Wang, A. Karki, A. T. Lill, G. C. Bazan, T. Q. Nguyen, *ACS Nano* **2018**, *12*, 3938.
[100] M. Nikolka, I. Nasrallah, B. Rose, M. K. Ravva, K. Broch, A. Sadhanala, D. Harkin, J. Charmet, M. Hurhangee, A. Brown, S. Illig, P. Too, J. Jongman, I. McCulloch, J. L. Bredas, H. Sirringhaus, *Nat. Mater.* **2017**, *16*, 356.
[101] H. Phan, M. J. Ford, A. T. Lill, M. Wang, G. C. Bazan, T. Q. Nguyen, *Adv. Funct. Mater.* **2017**, *27*, 1701358.
[102] K. Yu, J. M. Lee, J. Kim, G. Kim, H. Kang, B. Park, Y. Ho Kahng, S. Kwon, S. Lee, B. H. Lee, J. Kim, H. I. Park, S. O. Kim, K. Lee, *Nano Lett.* **2014**, *14*, 7100.
[103] H. L. Wang, Z. N. Bao, *Nano Today* **2015**, *10*, 737.
[104] T. Lei, I. Pochorovski, Z. Bao, *Acc. Chem. Res.* **2017**, *50*, 1096.
[105] D. Fong, A. Adronov, *Chem. Sci.* **2017**, *8*, 7292.
[106] M. Wang, F. Jakubka, F. Gannott, M. Schweiger, J. Zaumseil, *Org. Electron.* **2014**, *15*, 809.
[107] C. Smithson, Y. L. Wu, T. Wigglesworth, S. Gardner, S. P. Zhu, H. Y. Nie, *Org. Electron.* **2014**, *15*, 2639.
[108] M. Qu, H. Li, R. Liu, S. L. Zhang, Z. J. Qiu, *Nat. Commun.* **2014**, *5*, 3185.
[109] J. Huang, A. L. Ng, Y. Piao, C. F. Chen, A. A. Green, C. F. Sun, M. C. Hersam, C. S. Lee, Y. Wang, *J. Am. Chem. Soc.* **2013**, *135*, 2306.
[110] Y. L. Chu, X. H. Wu, J. Du, J. Huang, *RSC Adv.* **2017**, *7*, 30626.
[111] G. W. Hsieh, J. Y. Wu, K. Ogata, K. Y. Cheng, *Org. Electron.* **2016**, *35*, 158.
[112] S. Y. Lin, C. Y. Chan, C. W. Tsai, G. W. Hsieh, *Org. Electron.* **2018**, *57*, 269.
[113] F. C. Liu, W. L. Chow, X. X. He, P. Hu, S. J. Zheng, X. L. Wang, J. D. Zhou, Q. D. Fu, W. Fu, P. Yu, Q. S. Zeng, H. J. Fan, B. K. Tay, C. Kloc, Z. Liu, *Adv. Funct. Mater.* **2015**, *25*, 5865.
[114] R. Mas-Balleste, C. Gomez-Navarro, J. Gomez-Herrero, F. Zamora, *Nanoscale* **2011**, *3*, 20.
[115] S. Z. Butler, S. M. Hollen, L. Cao, Y. Cui, J. A. Gupta, H. R. Gutierrez, T. F. Heinz, S. S. Hong, J. Huang, A. F. Ismach, E. Johnston-Halperin, M. Kuno, V. V. Plashnitsa, R. D. Robinson, R. S. Ruoff, S. Salahuddin, J. Shan, L. Shi, M. G. Spencer, M. Terrones, W. Windl, J. E. Goldberger, *ACS Nano* **2013**, *7*, 2898.
[116] C. Li, Q. Cao, F. Wang, Y. Xiao, Y. Li, J. J. Delaunay, H. Zhu, *Chem. Soc. Rev.* **2018**, *47*, 4981.
[117] G. Fiori, F. Bonaccorso, G. Iannaccone, T. Palacios, D. Neumaier, A. Seabaugh, S. K. Banerjee, L. Colombo, *Nat. Nanotechnol.* **2014**, *9*, 768.
[118] K. S. Novoselov, A. Mishchenko, A. Carvalho, A. H. Castro Neto, *Science* **2016**, *353*, aac9439.
[119] D. Jariwala, T. J. Marks, M. C. Hersam, *Nat. Mater.* **2017**, *16*, 170.
[120] Y. L. Huang, Y. J. Zheng, Z. Song, D. Chi, A. T. S. Wee, S. Y. Quek, *Chem. Soc. Rev.* **2018**, *47*, 3241.
[121] Q. Ren, Q. Xu, H. Xia, X. Luo, F. Zhao, L. Sun, Y. Li, W. Lv, L. Du, Y. Peng, Z. Zhao, *Org. Electron.* **2017**, *51*, 142.
[122] X. He, W. Chow, F. Liu, B. Tay, Z. Liu, *Small* **2017**, *13*, 1602558.
[123] D. Jariwala, S. L. Howell, K. S. Chen, J. Kang, V. K. Sangwan, S. A. Filippone, R. Turrisi, T. J. Marks, L. J. Lauhon, M. C. Hersam, *Nano Lett.* **2016**, *16*, 497.
[124] X. Y. Yu, A. Rahmanudin, X. A. Jeanbourquin, D. Tsokkou, N. Guijarro, N. Banerji, K. Sivula, *ACS Energy Lett.* **2017**, *2*, 524.
[125] X. Zhang, J. Mao, W. Deng, X. Xu, L. Huang, X. Zhang, S. T. Lee, J. Jie, *Adv. Mater.* **2018**, *30*, 1800187.
[126] Y. Yao, L. Zhang, T. Leydecker, P. Samori, *J. Am. Chem. Soc.* **2018**, *140*, 6984.
[127] Q. Li, S. Ding, W. Zhu, L. Feng, H. Dong, W. Hu, *J. Mater. Chem. C* **2016**, *4*, 9388.

[128] J. Soeda, Y. Hirose, M. Yamagishi, A. Nakao, T. Uemura, K. Nakayama, M. Uno, Y. Nakazawa, K. Takimiya, J. Takeya, *Adv. Mater.* **2011**, *23*, 3309.
[129] W. Deng, X. Zhang, L. Wang, J. Wang, Q. Shang, X. Zhang, L. Huang, J. Jie, *Adv. Mater.* **2015**, *27*, 7305.
[130] X. Zhang, J. Jie, W. Deng, Q. Shang, J. Wang, H. Wang, X. Chen, X. Zhang, *Adv. Mater.* **2016**, *28*, 2475.
[131] W. Deng, X. Zhang, X. Zhang, J. Guo, J. Jie, *Adv. Mater. Technol.* **2017**, *2*, 1600280.
[132] C. Fan, A. P. Zoombelt, H. Jiang, W. Fu, J. Wu, W. Yuan, Y. Wang, H. Li, H. Chen, Z. Bao, *Adv. Mater.* **2013**, *25*, 5762.
[133] S. Vasimalla, N. V. V. Subbarao, P. K. Iyer, *J. Mater. Chem. C* **2016**, *4*, 7102.
[134] K. Kobashi, R. Hayakawa, T. Chikyow, Y. Wakayama, *Adv. Electron. Mater.* **2017**, *3*, 1700106.
[135] K. Kobashi, R. Hayakawa, T. Chikyow, Y. Wakayama, *Nano Lett.* **2018**, *18*, 4355.
[136] J. Wu, C. Fan, G. Xue, T. Ye, S. Liu, R. Lin, H. Chen, H. L. Xin, R. G. Xiong, H. Li, *Adv. Mater.* **2015**, *27*, 4476.
[137] X. J. She, D. Gustafsson, H. Sirringhaus, *Adv. Mater.* **2017**, *29*, 1604769.
[138] J. Kim, D. Khim, J. S. Yeo, M. Kang, K. J. Baeg, D. Y. Kim, *Adv. Opt. Mater.* **2017**, *5*, 1700655.
[139] A. F. Paterson, N. D. Treat, W. Zhang, Z. Fei, G. Wyatt-Moon, H. Faber, G. Vourlias, P. A. Patsalas, O. Solomeshch, N. Tessler, M. Heeney, T. D. Anthopoulos, *Adv. Mater.* **2016**, *28*, 7791.
[140] I. Isakov, A. F. Paterson, O. Solomeshch, N. Tessler, Q. Zhang, J. Li, X. Zhang, Z. Fei, M. Heeney, T. D. Anthopoulos, *Appl. Phys. Lett.* **2016**, *109*, 263301.
[141] T. Leydecker, M. Herder, E. Pavlica, G. Bratina, S. Hecht, E. Orgiu, P. Samori, *Nat. Nanotechnol.* **2016**, *11*, 769.
[142] M. Alt, M. Jesper, J. Schinke, S. Hillebrandt, P. Reiser, T. Rodlmeier, I. Angelova, K. Deing, T. Glaser, E. Mankel, W. Jaegermann, A. Pucci, U. Lemmer, U. H. F. Bunz, W. Kowalsky, G. Hernandez-Sosa, R. Lovrincic, M. Hamburger, *Adv. Funct. Mater.* **2016**, *26*, 3172.
[143] H. T. Zhang, H. L. Chen, W. Ma, J. S. Hui, S. Meng, W. Xu, D. B. Zhu, X. F. Guo, *J. Mater. Chem. C* **2016**, *4*, 5289.
[144] J. C. Love, L. A. Estroff, J. K. Kriebel, R. G. Nuzzo, G. M. Whitesides, *Chem. Rev.* **2005**, *105*, 1103.
[145] W. Huang, Y. H. Lin, T. D. Anthopoulos, *ACS Appl. Mater. Interfaces* **2018**, *10*, 10202.
[146] X. Y. Cheng, Y. Y. Noh, J. P. Wang, M. Tello, J. Frisch, R. P. Blum, A. Vollmer, J. P. Rabe, N. Koch, H. Sirringhaus, *Adv. Funct. Mater.* **2009**, *19*, 2407.
[147] M. R. Niazi, R. P. Li, M. Abdelsamie, K. Zhao, D. H. Anjum, M. M. Payne, J. Anthony, D. M. Smilgies, A. Amassian, *Adv. Funct. Mater.* **2016**, *26*, 2371.
[148] T. Mosciatti, M. G. Del Rosso, M. Herder, J. Frisch, N. Koch, S. Hecht, E. Orgiu, P. Samori, *Adv. Mater.* **2016**, *28*, 6606.
[149] T. Kanagasekaran, H. Shimotani, R. Shimizu, T. Hitosugi, K. Tanigaki, *Nat. Commun.* **2017**, *8*, 999.
[150] C. G. Tang, M. C. Ang, K. K. Choo, V. Keerthi, J. K. Tan, M. N. Syafiqah, T. Kugler, J. H. Burroughes, R. Q. Png, L. L. Chua, P. K. Ho, *Nature* **2016**, *539*, 536.
[151] W. L. Seah, C. G. Tang, R. Q. Png, V. Keerthi, C. Zhao, H. Guo, J. G. Yang, M. Zhou, P. K. H. Ho, L. L. Chua, *Adv. Funct. Mater.* **2017**, *27*, 1606291.
[152] Y. Cao, S. Liu, Q. Shen, K. Yan, P. J. Li, J. Xu, D. P. Yu, M. L. Steigerwald, C. Nuckolls, Z. F. Liu, X. F. Guo, *Adv. Funct. Mater.* **2009**, *19*, 2743.
[153] B. Sun, C. H. Zhu, Y. Liu, C. Wang, L. J. Wan, D. Wang, *Chem. Mater.* **2017**, *29*, 4367.
[154] C.-H. Kim, I. Kymissis, *J. Mater. Chem. C* **2017**, *5*, 4598.
[155] S. Parui, M. Ribeiro, A. Atxabal, R. Llopis, F. Casanova, L. E. Hueso, *Nanoscale* **2017**, *9*, 10178.
[156] B. Kang, S. K. Lee, J. Jung, M. Joe, S. B. Lee, J. Kim, C. Lee, K. Cho, *Adv. Mater.* **2018**, *30*, 1706480.
[157] H. A. Becerril, R. M. Stoltenberg, M. L. Tang, M. E. Roberts, Z. Liu, Y. Chen, D. H. Kim, B. L. Lee, S. Lee, Z. Bao, *ACS Nano* **2010**, *4*, 6343.
[158] Y. J. Choi, J. S. Kim, J. Y. Cho, H. J. Woo, J. Yang, Y. J. Song, M. S. Kang, J. T. Han, J. H. Cho, *Chem. Mater.* **2018**, *30*, 636.
[159] O. Fenwick, C. Van Dyck, K. Murugavel, D. Cornil, F. Reinders, S. Haar, M. Mayor, J. Cornil, P. Samorì, *J. Mater. Chem. C* **2015**, *3*, 3007.
[160] S. Choi, C. Fuentes-Hernandez, C.-Y. Wang, T. M. Khan, F. A. Larrain, Y. Zhang, S. Barlow, S. R. Marder, B. Kippelen, *ACS Appl. Mater. Interfaces* **2016**, *8*, 24744.
[161] A. Petritz, M. Krammer, E. Sauter, M. Gärtner, G. Nascimbeni, B. Schrode, A. Fian, H. Gold, A. Cojocaru, E. Karner-Petritz, R. Resel, A. Terfort, E. Zojer, M. Zharnikov, K. Zojer, B. Stadlober, *Adv. Funct. Mater.28*, **2018**, 1804462.
[162] J. Roh, T. Lee, C.-m. Kang, J. Kwak, P. Lang, G. Horowitz, H. Kim, C. Lee, *Sci. Rep.* **2017**, *7*, 46365.
[163] S. Choi, C. Fuentes-Hernandez, C. Y. Wang, T. M. Khan, F. A. Larrain, Y. Zhang, S. Barlow, S. R. Marder, B. Kippelen, *ACS Appl. Mater. Interfaces* **2016**, *8*, 24744.
[164] X. Zhuang, W. Huang, S. Han, Y. Jiang, H. Zheng, J. Yu, *Org. Electron.* **2017**, *49*, 334.
[165] Y. Gao, Y. Shi, H. Meng, X. Wang, *Org. Electron.* **2018**, *62*, 248.
[166] J.-L. Hou, D. Kasemann, J. Widmer, A. A. Günther, B. Lüssem, K. Leo, *Appl. Phys. Lett.* **2016**, *108*, 103303.
[167] D. Panigrahi, S. Kumar, A. Dhar, *Appl. Phys. Lett.* **2017**, *111*, 173501.
[168] H. Karimi-Alavijeh, A. Ehsani, *Thin Solid Films* **2015**, *590*, 214.
[169] X. Chen, X. Wei, H. Zhang, J. Wang, *Phys. Status Solidi A* **2017**, *214*, 1700064.
[170] L. He, D. Ji, E. Wang, Y. Zhen, H. Dong, W. Hu, *Sci. China: Chem.* **2015**, *58*, 1027.
[171] D. X. Long, Y. Xu, H. X. Wei, C. Liu, Y. Y. Noh, *Phys. Chem. Chem. Phys.* **2015**, *17*, 20160.
[172] B. Sun, C.-H. Zhu, Y. Liu, C. Wang, L.-J. Wan, D. Wang, *Chem. Mater.* **2017**, *29*, 4367.
[173] J. Y. Choi, W. Kang, B. Kang, W. Cha, S. K. Son, Y. Yoon, H. Kim, Y. Kang, M. J. Ko, H. J. Son, K. Cho, J. H. Cho, B. Kim, *ACS Appl. Mater. Interfaces* **2015**, *7*, 6002.
[174] Y. H. Lee, M. Jang, M. Y. Lee, O. Y. Kweon, J. H. Oh, *Chemistry* **2017**, *3*, 724.
[175] Y. P. Zang, F. J. Zhang, C. A. Di, D. B. Zhu, *Mater. Horiz.* **2015**, *2*, 140.
[176] S. C. Mannsfeld, B. C. Tee, R. M. Stoltenberg, C. V. Chen, S. Barman, B. V. Muir, A. N. Sokolov, C. Reese, Z. Bao, *Nat. Mater.* **2010**, *9*, 859.
[177] Y. Zang, F. Zhang, D. Huang, X. Gao, C. A. Di, D. Zhu, *Nat. Commun.* **2015**, *6*, 6269.
[178] H. Zhang, X. Guo, J. Hui, S. Hu, W. Xu, D. Zhu, *Nano Lett.* **2011**, *11*, 4939.
[179] Y. Zang, F. Zhang, D. Huang, C. A. Di, D. Zhu, *Adv. Mater.* **2015**, *27*, 7979.
[180] T. Shaymurat, Q. Tang, Y. Tong, L. Dong, Y. Liu, *Adv. Mater.* **2013**, *25*, 2269.
[181] W. Huang, X. Zhuang, F. S. Melkonyan, B. Wang, L. Zeng, G. Wang, S. Han, M. J. Bedzyk, J. Yu, T. J. Marks, A. Facchetti, *Adv. Mater.* **2017**, *29*, 1701706.
[182] L. Torsi, M. Magliulo, K. Manoli, G. Palazzo, *Chem. Soc. Rev.* **2013**, *42*, 8612.
[183] C. Zhang, P. Chen, W. Hu, *Chem. Soc. Rev.* **2015**, *44*, 2087.
[184] F. Zhang, C. A. Di, N. Berdunov, Y. Hu, Y. Hu, X. Gao, Q. Meng, H. Sirringhaus, D. Zhu, *Adv. Mater.* **2013**, *25*, 1401.
[185] Z. Wang, L. Huang, X. Zhu, X. Zhou, L. Chi, *Adv. Mater.* **2017**, *29*, 1703192.

[186] Y. Ohko, T. Tatsuma, T. Fujii, K. Naoi, C. Niwa, Y. Kubota, A. Fujishima, *Nat. Mater.* **2003**, *2*, 29.
[187] M. R. Hoffmann, S. T. Martin, W. Choi, D. W. Bahnemann, *Chem. Rev.* **1995**, *95*, 69.
[188] S. Liu, J. Li, Q. Shen, Y. Cao, X. Guo, G. Zhang, C. Feng, J. Zhang, Z. Liu, M. L. Steigerwald, D. Xu, C. Nuckolls, *Angew. Chem., Int. Ed.* **2009**, *48*, 4759.
[189] J. Wang, F. Shen, Z. Wang, G. He, J. Qin, N. Cheng, M. Yao, L. Li, X. Guo, *Angew. Chem., Int. Ed.* **2014**, *53*, 5038.
[190] H. Wen, W. Li, J. Chen, G. He, L. Li, M. A. Olson, A. C. Sue, J. F. Stoddart, X. Guo, *Sci. Adv.* **2016**, *2*, e1601113.
[191] B. Tian, T. Cohen-Karni, Q. Qing, X. Duan, P. Xie, C. M. Lieber, *Science* **2010**, *329*, 830.
[192] S. Sorgenfrei, C. Y. Chiu, R. L. Gonzalez, Jr., Y. J. Yu, P. Kim, C. Nuckolls, K. L. Shepard, *Nat. Nanotechnol.* **2011**, *6*, 126.
[193] J. Larkin, R. Y. Henley, V. Jadhav, J. Korlach, M. Wanunu, *Nat. Nanotechnol.* **2017**, *12*, 1169.
[194] K. S. Novoselov, V. I. Fal'ko, L. Colombo, P. R. Gellert, M. G. Schwab, K. Kim, *Nature* **2012**, *490*, 192.
[195] Y. Liu, X. Dong, P. Chen, *Chem. Soc. Rev.* **2012**, *41*, 2283.
[196] W. Yuan, G. Shi, *J. Mater. Chem. A* **2013**, *1*, 10078.
[197] B. Cho, J. Yoon, M. G. Hahm, D. H. Kim, A. R. Kim, Y. H. Kahng, S. W. Park, Y. J. Lee, S. G. Park, J. D. Kwon, C. S. Kim, M. Song, Y. Jeong, K. S. Nam, H. C. Ko, *J. Mater. Chem. C* **2014**, *2*, 5280.
[198] W. Yuan, L. Huang, Q. Zhou, G. Shi, *ACS Appl. Mater. Interfaces* **2014**, *6*, 17003.
[199] D. Zhang, L. Gan, Y. Cao, Q. Wang, L. Qi, X. Guo, *Adv. Mater.* **2012**, *24*, 2715.
[200] L. Gan, J. Zhou, F. Ke, H. Gu, D. N. Li, Z. H. Hu, Q. Sun, X. F. Guo, *NPG Asia Mater.* **2012**, *4*, e31.
[201] L. Gan, D. Zhang, X. Guo, *Small* **2012**, *8*, 1326.
[202] L. Britnell, R. M. Ribeiro, A. Eckmann, R. Jalil, B. D. Belle, A. Mishchenko, Y. J. Kim, R. V. Gorbachev, T. Georgiou, S. V. Morozov, A. N. Grigorenko, A. K. Geim, C. Casiraghi, A. H. Castro Neto, K. S. Novoselov, *Science* **2013**, *340*, 1311.
[203] H. Zhou, Q. Chen, G. Li, S. Luo, T. B. Song, H. S. Duan, Z. Hong, J. You, Y. Liu, Y. Yang, *Science* **2014**, *345*, 542.
[204] J. B. Sambur, T. Novet, B. A. Parkinson, *Science* **2010**, *330*, 63.